**SANDIA REPORT**
SAND2009-7718
Unlimited Release
Printed November 2009

# Multilayer Co-Extrusion Technique for Developing High Energy Density Organic Devices

Lisa Mondy, Randy Mrozek, Rekha Rao, Joseph Lenhart, Lothar Bieg, Scott Spangler, Duane Schneider, Mark Stavig, John Schroeder, Mike Winter, Phillip Cole

Prepared by
Sandia National Laboratories
Albuquerque, New Mexico 87185 and Livermore, California 94550

Sandia is a multiprogram laboratory operated by Sandia Corporation,
a Lockheed Martin Company, for the United States Department of Energy's
National Nuclear Security Administration under Contract DE-AC04-94AL85000.



Issued by Sandia National Laboratories, operated for the United States Department of Energy by Sandia Corporation.



Available to DOE and DOE contractors from
U.S. Department of Energy
Office of Scientific and Technical Information
P.O. Box 62
Oak Ridge, TN 37831

Telephone: (865) 576-8401
Facsimile: (865) 576-5728
E-Mail: reports@adonis.osti.gov
Online ordering: http://www.osti.gov/bridge

Available to the public from
U.S. Department of Commerce
National Technical Information Service
5285 Port Royal Rd.
Springfield, VA 22161

Telephone: (800) 553-6847
Facsimile: (703) 605-6900
E-Mail: orders@ntis.fedworld.gov
Online order: http://www.ntis.gov/help/ordermethods.asp?loc=7-4-0#online

SAND2009-7718
Unlimited Release
Printed November 2009

# Multilayer Co-Extrusion Technique for Developing High Energy Density Organic Devices

Lisa Mondy[1], Randy Mrozek[7], Rekha Rao[1], Joseph Lenhart[7], Lothar Bieg[2], Scott Spangler[3], Duane Schneider[4], Mark Stavig[5], John Schroeder[5], Mike Winter[6], Phillip Cole[8]

[1]Thermal and Fluid, MS0346
[2] Frequency Devices, Capacitors and Magnetics, MS
[3]Organic Materials, MS0958
[4]CINT Science, MS1305
[5]Organic Materials, MS0888
[6]Ceramic and Glass, MS1245
Sandia National Laboratories
P.O. Box 5800
Albuquerque, New Mexico 87185

[7]Army Research Lab
Weapon and Material Research Directorate
Adelphi, MD 20783-1197

[8] Northrop-Grumman
Herndon, VA 20171

**Abstract**

The purpose of this project is to develop multi-layered co-extrusion (MLCE) capabilities at Sandia National Laboratories to produce multifunctional polymeric structures. Multi-layered structures containing layers of alternating electrical, mechanical, optical, or structural properties can be applied to a variety of potential applications including energy storage, optics, sensors, mechanical, and barrier applications relevant to the internal and external community. To obtain the desired properties, fillers must be added to the polymer materials that are much smaller than the end layer thickness. We developed two filled polymer systems, one for conductive layers and one for dielectric layers and demonstrated the potential for using MLCE to manufacture capacitors. We also developed numerical models to help determine the material and processing parameters that impact processing and layer stability.

## ACKNOWLEDGMENTS

The authors would like to acknowledge useful discussions with Randy Schunk, David Noble, Anne Grillet, and Chris Diantonio, as well as Alice Kilgo's help with imaging, and Adam Lester's help in capacitance measurements. This work was supported by the Laboratory Directed Research and Development program at Sandia National Laboratories.

# CONTENTS



# FIGURES

# 1 INTRODUCTION

The goal of this project was to develop multi-layer co-extrusion capabilities at Sandia National Laboratories to produce continuous layered devices. Multi-layered co-extrusion combines multiple polymers into a layered structure to produce composite properties that are not found in a single polymer. Specifically, multi-layered structures with alternating mechanical, electrical, or optical properties can be produced to enable a variety of functional devices [Khomenko et al. 2005, Gerard et al. 2002, Chung 2001]. For example, multi-layered structures have found commercial application in the area of food and beverage packaging for their barrier properties or as protective coatings. Multi-layered structures have also been produced that act similarly to a double paned window to maintain the temperature of contents for extended transport. There are also several emerging technologies that could potentially benefit from multi-layered structures including energy storage devices, sensors, optical devices, barrier materials, membranes, microcomposites, or armor applications.

Multi-layered structures can be produced by a couple of methods. The polymer flows can be combined from multiple extruders into a layered structure (Figure 1). Multi-layered structures produced by this method are limited in the number of layers and layer thickness by the die design. In contrast, the equipment developed in this project combines the polymer flows from two extruders into an initial layered structure that then passes through a series of dies to multiply the number of layers (Figure 2). The first die splits the flow vertically, the two components are stacked, and recombined to effectively double the number of layers. As the number of layers is increased in the same die cross-sectional area the individual layer thickness also decreases. This method has successfully been implemented by companies like 3M and Dow to produce multilayered structures of ~ 20 μm and 110 nm, respectively [3M 2005, Dow 2007].

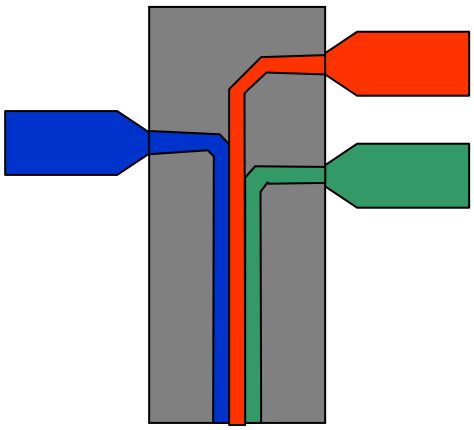

**Figure 1. Multi-layered structure produced by combining multiple polymer flows into a layered structure.**

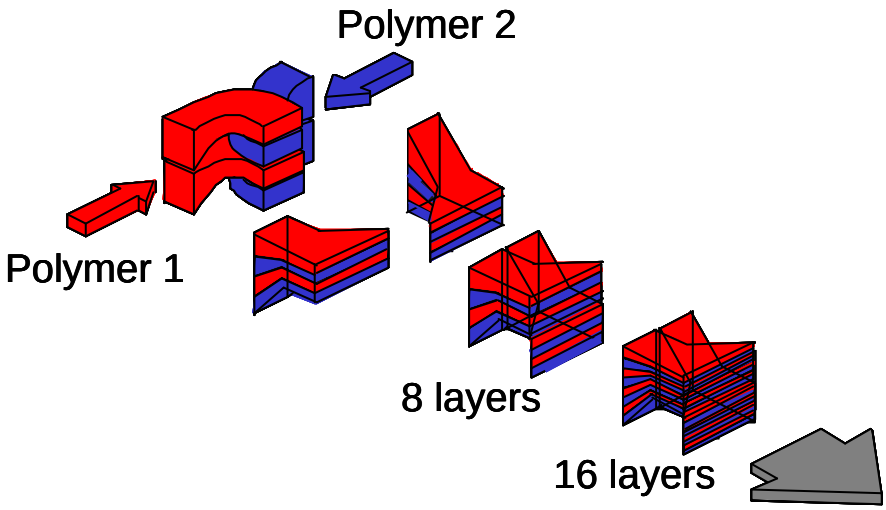


**Figure 2. Multi-layered die system that multiplies the number of layers in a given cross-section**

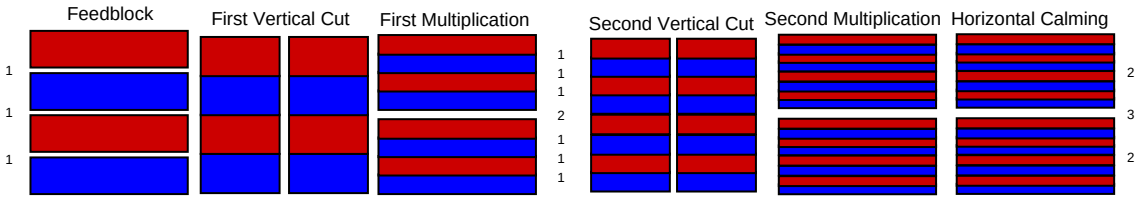


**Figure 3. Schematic of multiplication scheme.**

The multi-layer co-extrusion equipment now at Sandia is based on equipment from the Macosko group at the University of Minnesota; however, we have modified some limitations of the original equipment. [Zhao & Macosko 2002]. A circular external die shape was used to facilitate more uniform heating with a band heater rather than the previous square design. In addition, a "calming section" was added after each multiplication to provide flow stability. Finally, the initial layered structure consisted of 8 layers rather than 4 to decrease the number of multiplications needed (Figure 4). As a result, the number of multiplication sections, n, will result in $2^{n+3}$ layers in a 1 mm tape. In theory, these layers should not intermix provided there is a uniform laminar flow. However, instabilities, especially as the layers get thinner, can lead to non-uniformity of the layers or even layer break up.

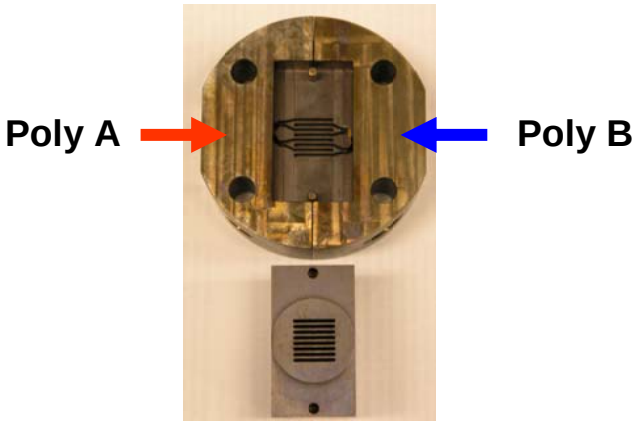


**Figure 4. Picture of the die used to produce the initial eight layered structure.**

As the material exits the die area, it goes through the sheeting section where the initially square cross-section of the die is drawn down to a thin sheet of the same initial cross-section.

This is done with two converging dies to flatten and widen the extrudate ribbon. After the drawdown, the still hot ribbon is pulled through chilled rollers to freeze the structure. A sketch and a photo of the co-extrusion parts are shown in Figure 5.

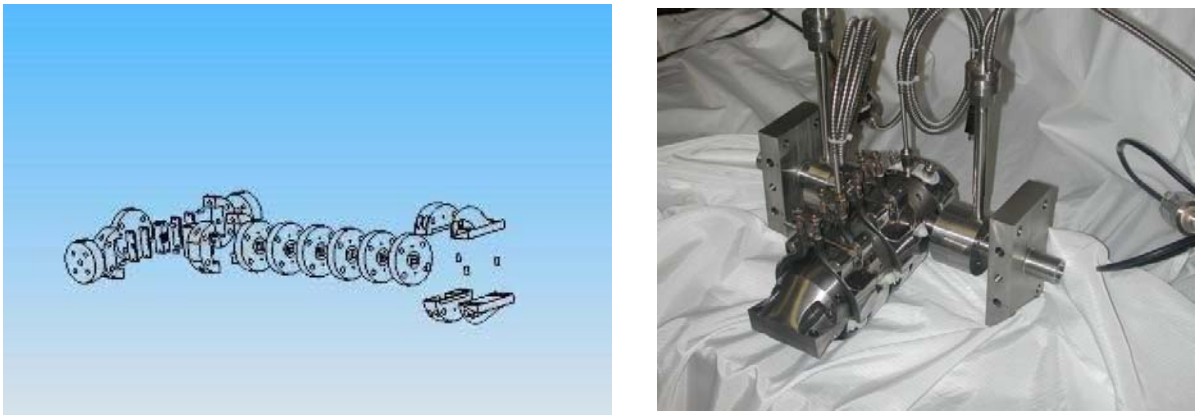

**Figure 5. Sketch and photo of the co-extrusion dies.**

The incorporation of filled materials into the layered structures will increase the versatility and applicability of the technique to aid some of the emerging technologies. As is the case for filled bulk materials, the incorporation of fillers can enhance the material properties of the matrix including the thermal stability, flame retardency, chemical resistance, permeability, conductivity, and stiffness. The targeted application is to extrude a capacitor structure consisting of alternating conductive and non-conductive layers (Figure 6).

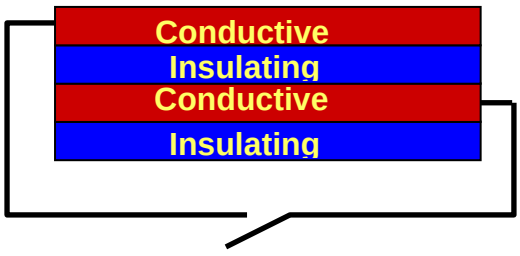


**Figure 6. Schematic of the layered capacitor structure.**

In the next section (Section 2) we describe initial testing of the equipment with unfilled polymers. In the following section (Section 3) we report the efforts to develop conductive thermoplastic polymers suitable for co-extrusion. We describe processing and properties of the several materials made with various conductive fillers, including discussion of mixing methods with single and twin screw extruders, the results of processing tests at various temperatures and flow rates, and preliminary viscosity measurements. Here we discuss the novel idea to include a low-melting-point eutectic as a conductive filler. The conductivity of the various materials are also reported. Development of a dielectric-filled polymer is outlined in Section 4. Next, in Section 5, we detail the rheology of the filled polymers selected to prototype a co-extruded capacitor. The co-extrusion of filled polymers to produce a prototype capacitor is described in Section 6. In Section 7, we discuss the development of numerical processing models to help determine the conditions necessary to minimize instabilities that can result in poor layer formation. Here we report some model validation experiments using lightly filled polymers, as well as predictions for the behavior of co-extruded materials that are mismatched in density or viscosity. In the final section we summarize the difficulties and challenges still associated with co-extrusion of filled systems in general and with the development of co-extruded capacitors in particular.

# 2 CO-EXTRUSION PROCESSING WITH UNFILLED POLYMERS

To verify the equipment, layered structures consisting of polystyrene and polyethylene were produced. The initial structures consisted of 8, 16, and 32 layers or 0, 1, and 2 multiplication sections. An unexpected aspect of these initial films is that the overall film thickness is far less than 1 mm and closer to 350 μm (Figure 7). This is most likely because of the larger than optimum distance between the take up roller and the extrusion port. This effect will be reduced as the number of dies is increased resulting in the die channel lengthening and eliminating the physical constraints of the equipment. A thinner film results in an individual layer thickness on the order of 10s of microns with reasonable uniformity considering these films were not optimized in terms of viscosities and interfacial properties.

The dark voids in Figure 7b are due to delamination during the sample preparation for the imaging process. This is a result of the poor adhesion between polystyrene and polyethylene and not poor layer formation. It is anticipated that similar polymer layers will exhibit less delamination and more uniform layer formation with better adhesion.

The initial layered structures demonstrated the effectiveness of the equipment, and the project focus was shifted to producing layered material where one or more of the layers are a filled composite, since optimizing the layer uniformity of unfilled polymers, although an active research area, was not the focus of the present work.

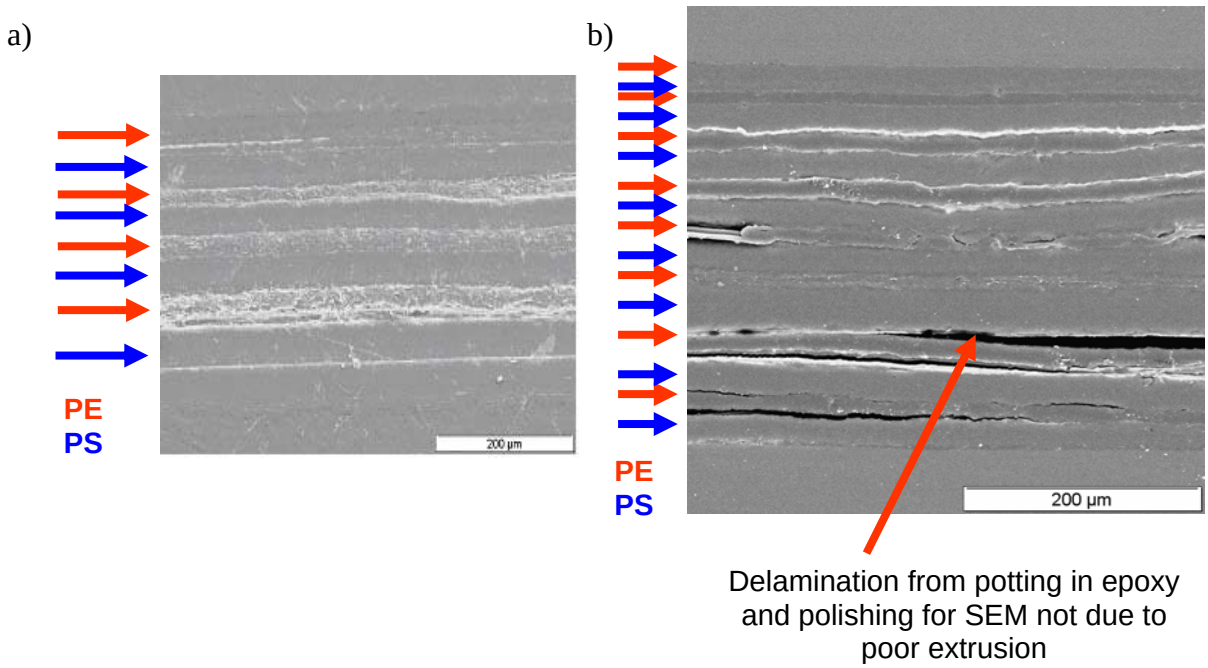


**Figure 7. SEM images of a) 8 and b) 16 layer structures consisting of alternating polyethylene and polystyrene.**

# 3 DEVELOPMENT OF A CONDUCTIVE POLYMER

## 3.1 Background

To produce a capacitor structure the biggest technical challenge is to produce a conductive polymer composite that is melt processable. Quite simply, if this problem cannot be resolved, a capacitor structure cannot be co-extruded.

Polymer conductivity has traditionally been obtained by two methods. First, an inherently conductive polymer can be used. However, these polymers typically consist of a conjugated backbone that is relatively rigid and will produce very high melt viscosities. In addition, the conjugated backbone will raise the melting point often above the degradation temperature of the polymer [Wessling 1998]. These factors make it difficult if not impossible to melt process. Because of this we decided to explore the addition of conductive fillers. Conductivity through incorporation of filler typically requires very high loadings. At these high loadings it can be difficult to disperse particles resulting in aggregation and inconsistent properties in the material. This issue could become worse as the particle size decreases, which must happen to facilitate a decrease in the layer thickness. More importantly, there is a dramatic increase in the viscosity at high loadings of solids.

To minimize the impact of filler loading, we also explored the addition of a low-melting-point eutectic to take advantage of the fact that emulsions in general have a lower viscosity than suspensions of solid particles at the same volume fraction of the dispersed phase. Figure 8 demonstrates the exponential increase in the viscosity as the volume fraction of spherical particles is increased, as well as the less dramatic effect of an emulsion where the viscosity of the dispersed phase is much lower than that of the continuous phase. The points in this figure are taken from the semi-empirical Krieger-Dougherty correlation for the relative viscosity of a suspension of solid particles [Krieger & Dougherty 1959]:

$$\frac{\eta_s}{\eta_0} = (1 - \frac{\phi}{\phi_m})^{-[\eta]\phi_m} \quad , \qquad \textbf{1}$$

where $\eta_s$ is the apparent viscosity of the suspension, $\eta_0$ is the viscosity of the continuous phase (the suspending medium), $\phi$ is the volume fraction of solids in suspension, $\phi_m$ is the maximum packing of solids, and [$\eta$] is the intrinsic viscosity of the suspension, which is defined as $\lim_{\phi \to 0} \frac{\eta_s - \eta_0}{\eta_0 \phi}$. Einstein showed that for hard spheres, [$\eta$] is 2.5 [Einstein 1906, 1911]. Here we take $\phi_m$ to be 0.65 and [$\eta$] to be 2.5, values that give a curve through Thomas' survey of suspension measurements [Thomas 1965].

Also plotted in Figure 8 are two formulas to describe the relative viscosity ($\eta_e/\eta_0$) of emulsions, where the droplet viscosity is much lower than that of the suspending phase. The Taylor-Mooney formulation [Taylor 1934, Mooney 1951, Prud'homme and Khan 1996] is:

$$\frac{\eta_e}{\eta_0} = \exp(\frac{K\phi_d}{1 - \phi_d}), \qquad \textbf{2}$$

where, for emulsions in which the viscosity ratio of the droplet viscosity to the continuous phase viscosity is zero, $K$=1, and $\phi_d$ is the volume fraction of droplets in the emulsion. Frankel and Acrivos [1970] proposed a more complex constitutive relationship that takes into account deformation of the droplets and gives rise to memory effects if surface tension is taken into effect. However, for finite concentrations but vanishing shear rates and viscosity ratios, the formula reduces to [Grizzutietal 1999]:

$$\frac{\eta_e}{\eta_0} = 1 + \phi_d + 2.5\phi_d^{\,2}. \qquad \textbf{3}$$

For high shear rates the viscosity is somewhat lower (again for vanishing viscosity ratio):

$$\frac{\eta_e}{\eta_0} = (1 + \phi_d + 2.5\phi_d{}^2)(\frac{3+12\phi_d}{3+20\phi_d}) \quad . \qquad \textbf{4}$$

From Figure 8, one can see that above a dispersed phase volume concentration of about 20%, the emulsion viscosity can be significantly lower than the suspension viscosity.

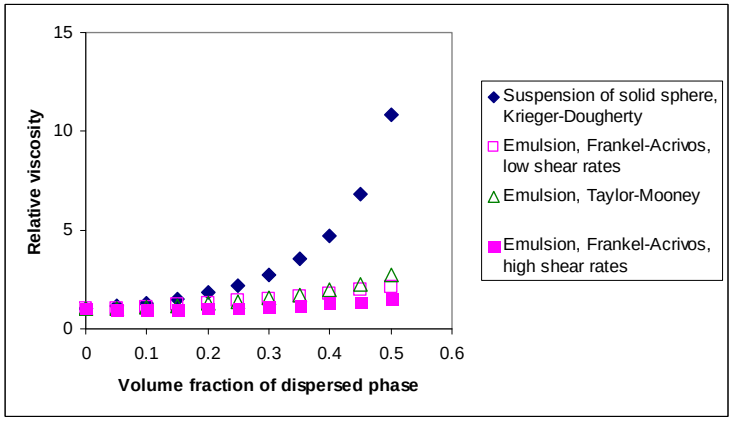


**Figure 8. Relative viscosity of suspensions of solids compared to emulsions of invisid drops.**

The various fillers and combinations we tried in order to develop a melt processable conductive polymer are described in the following subsections.

## 3.2 Micron Nickel Particulate Filler

To begin our studies of filled systems, we chose a nickel filler primarily due to its conductivity and relative stability to oxidation which is of particular importance to many Sandia applications. Most importantly, nickel is available in kilogram quantities in several sizes well into the sub-micron regime with narrow size distributions and good shape uniformity. We first examined a filler with a relatively large particle size because of its low price and good availability. Styron 666 polystyrene (Dow) was used as a matrix simply for availability, and any insight learned from this system should be readily transitioned to another matrix material.

The filler, 2-4 µm nickel particulate (Aldrich), was incorporated using a Randcastle RCP-0750 single-screw extruder at 260 ºC. The filler was added in small increments (~2 g filler/10 g polymer material) to avoid large increases in the viscosity in poorly mixed regions, possibly resulting in damage to the screw. To accommodate incremental filler addition, the extruded material was collected, pelletized, and re-extruded with additional filler. After complete addition of the particulate in 10 volume % increments, the material was re-pelletized and extruded three times to enhance uniformity. The nickel loading was verified using Thermogravimetric Analysis (TGA) (Figure 9). The retained mass is consistent with the nickel loading after the degradation of polymer. The mass increase at higher temperatures is attributed to nickel oxidation above 300 ºC.

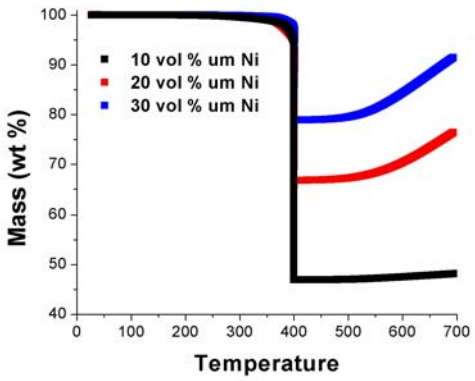


**Figure 9. TGA data for polystyrene loaded with 10, 20, and 30 vol % 2-4 µm nickel particulate.**

The composites were potted in epoxy, polished, and then imaged using a SEM (Figure 10). All of the samples contained large dark voids that are attributed to air entrainment as a result of the increased viscosity. At 30 volume % the material becomes nearly unprocessable. At this concentration the particles will congest the extrusion nozzle producing pressure buildup and failure of the burst disc.

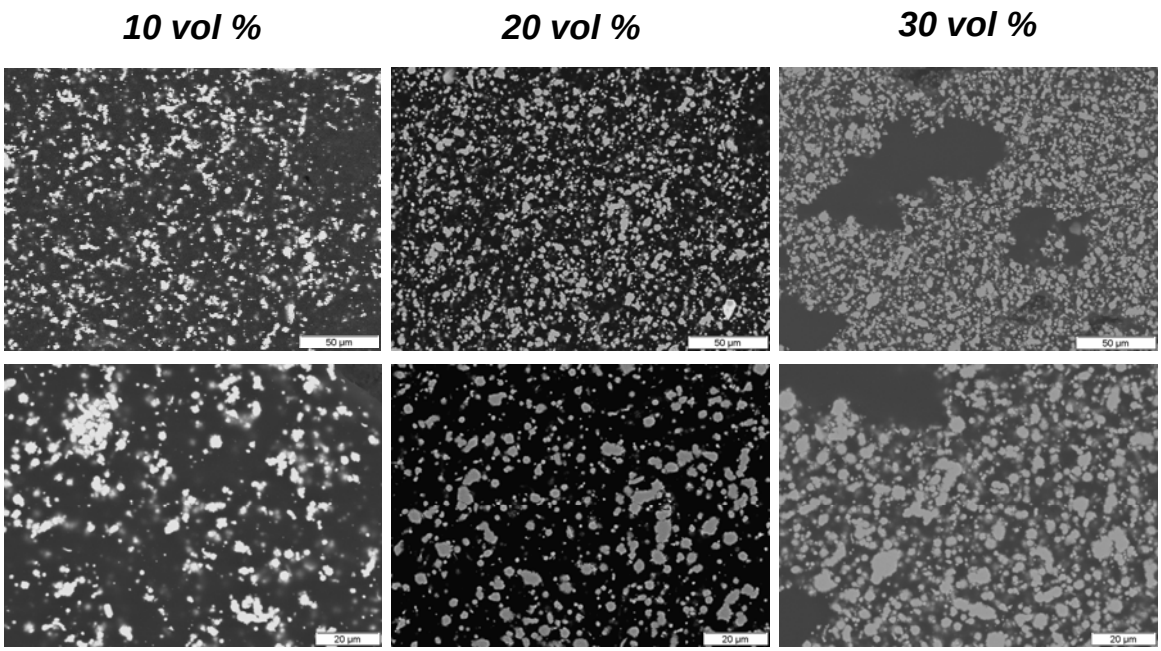


**Figure 10. SEM images of polystyrene loaded with 10, 20 and 30 vol % 2-4 μm nickel particulate. Dark areas are the polymer phase.**

The electrical properties of material at the various solids loadings were measured using a hand held multi-meter with alligator clip leads. The recorded resistance values were normalized to the distance between the leads. The 20 volume % sample had a resistance of ~ 100 kΩ/cm length and the resistance decreases to 2-4 Ω/cm length at 30 volume %.

## 3.3 Sub-micron Nickel Particulate Filler

With the 2-4 μm particles, layer thicknesses would be required to be no smaller than on the order of 10-100 μm to contain enough particles to be conductive. To facilitate producing thinner layers, we must use sub-micron fillers. The processing limitations of 200 nm spherical particulate (Nanodynamics) were also determined. The filler was added in the same manner as the larger filler. The retained mass in TGA was again consistent with the loading (Figure 11a). However, the TGA curve shape produced with these composites at higher temperatures was different than with the micron particles. This appears to be something fundamental to the particles as a TGA trace of the 200 nm nickel alone demonstrates a stable mass only below 360

ºC, above which temperature mass uptake proceeds (Figure 11b). We speculated that this could be caused by greater oxidation occurring because of the high surface area to volume ratio of the smaller particles.

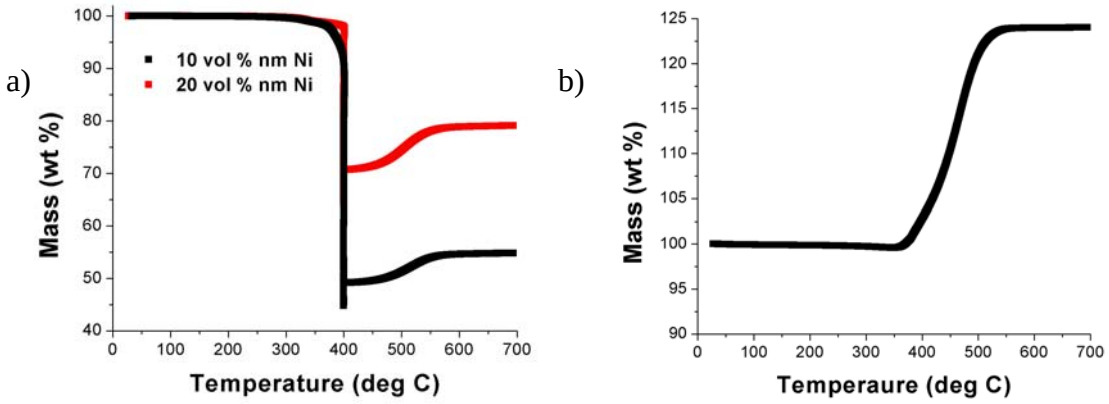


**Figure 11. TGA trace of a) 200 nm nickel loading in polystyrene and b) the 200 nm nickel particulate alone.**

In contrast to the larger particulate, processing difficulties did not manifest until 40 volume % loading. The SEMs reveal a dispersion that consists of well dispersed areas and areas of aggregation (Figure 12). Again, the dark regions in these materials are air voids that are attributed to the increase in viscosity. Unexpectedly, the material was not conductive even at 40 volume % loading.

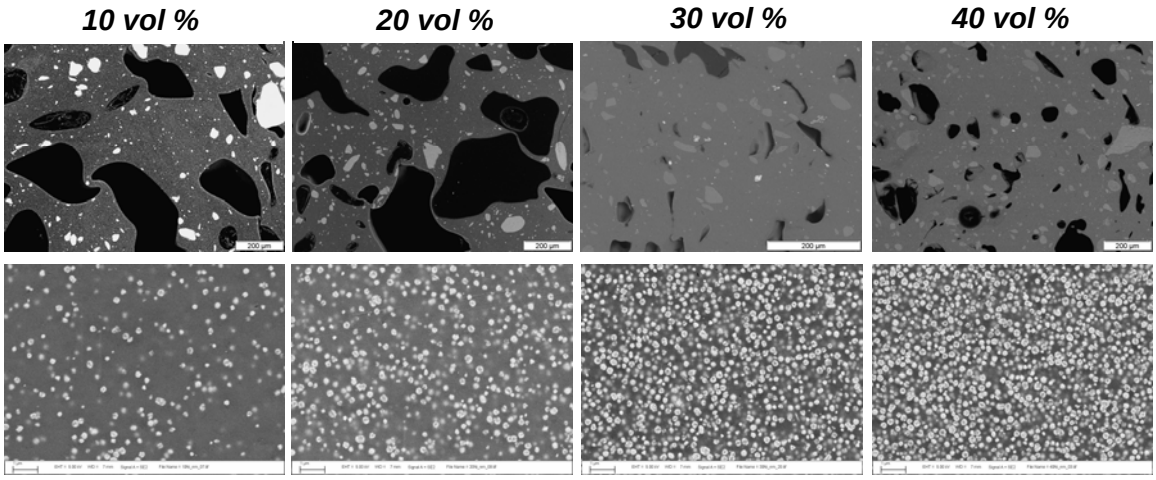


**Figure 12. SEM images of 10, 20, 30, and 40 volume % of 200 nm nickel particle loadings. Bottom images are high magnification images of well dispersed regions. Dark areas in the top images are voids.**

The lack of conductivity in the 200 nm nickel composites could be due to the aggregation increasing the relative percolation threshold or could be something unique to the specific material. The decreased dispersion in the 200 nm nickel is a common difficulty in sub-micron particle loaded composites. To aid the mixing, a new screw design was investigated that contained reflow sections (Figure 13). The materials were re-extruded through the extruders using the enhanced mixing times at variable speeds to determine impact of the screw design. Unfortunately, no apparent enhancement was observed with the new screw design other than the lifetime of the screw was dramatically reduced.

a)

b)

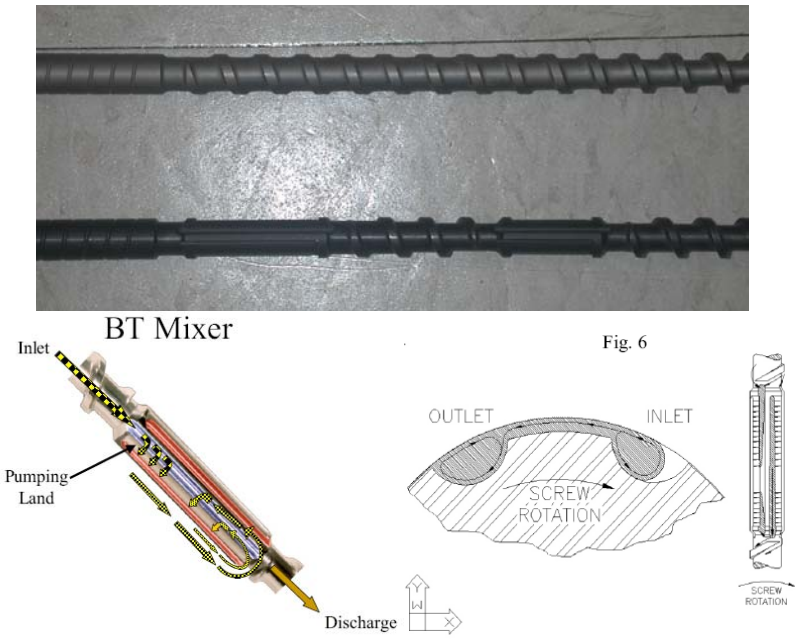


**Figure 13. a) Photograph and b) schematics of enhanced mixing sections used in the single screw extruder.**

To better determine if the mixing was having a significant impact on the percolation, high resolution images of a fracture surface from a 40 volume % 200 nm nickel particulate were taken (Figure 14). These images indicate that the particles were well dispersed outside of the aggregates. In addition, the aggregates did not appear to be fused, indicating that it may be possible to disperse them. It is also interesting to note that there were individual pockets of polymer. This indicates good particle dispersion with a thin layer of polymer around each particle. While this indicates good particle dispersion, it may actually be bad for conductivity where particle-particles contacts are ideal. However, the dispersion of particles overall appeared to be enough like that of the 2-4 μm nickel to anticipate percolation and conductivity. We decided to look at other possible reasons for the low conductivity.

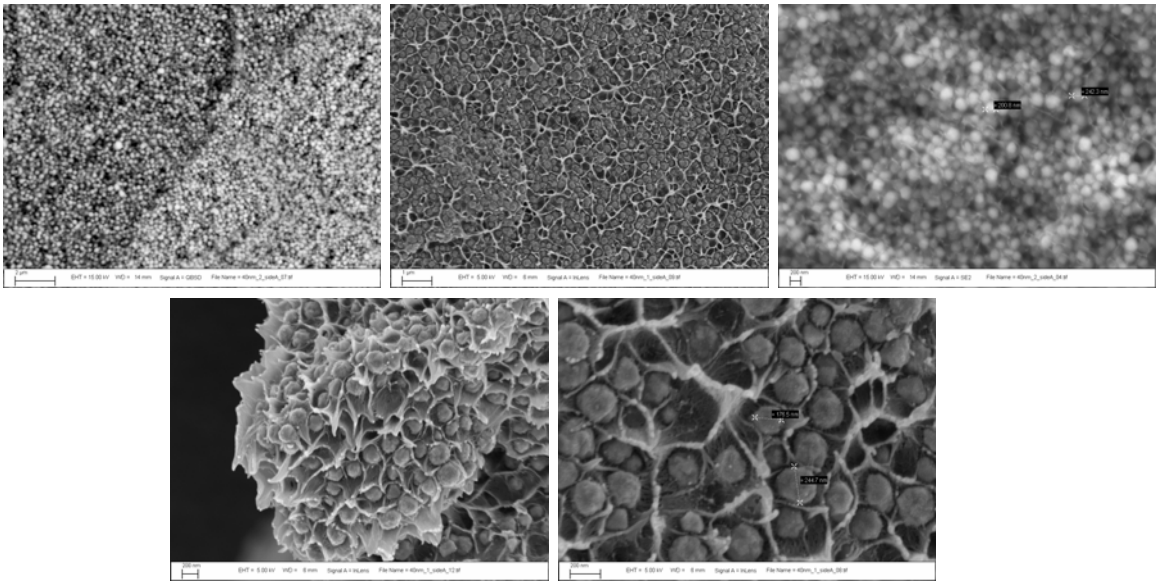

**Figure 14. High resolution SEM images of polystyrene containing 40 vol % 200 nm nickel particulate.**

EDS mapping of the oxygen during the high resolution SEM indicated that there was likely an oxide layer on the nickel (Figure 15). This could severely reduce the conductivity of the particles. To test this theory, we removed the oxide layer by treating the particles with 1 N HCl. There are two reactions that are likely to occur. The nickel oxide will be removed to form nickel chloride and water while the metallic nickel will form nickel chloride and hydrogen gas:

$$NiO_{(s)} + 2H^{+}_{(aq)} + 2Cl^{-}_{(aq)} \rightarrow Ni^{2+}_{(aq)} + 2Cl^{-}_{(aq)} + H_2O$$

$$Ni_{(s)} + 2H^{+}_{(aq)} + 2Cl^{-}_{(aq)} \rightarrow Ni^{2+}_{(aq)} + 2Cl^{-}_{(aq)} + H_{2(g)}$$

As a result, the progress of the reaction needs to be monitored to avoid significantly changing the shape and size uniformity. Figure 16 contains SEM images of the as-received materials and particulates treated for 2.5 and 4 h with 1 N HCl. After 2.5 hours the nickel particulate looks similar to the as-received material whereas after 4 hours the particles become faceted and are dramatically smaller. The conductivity was measured by placing the material between two copper sheets along with an insulating gasket to prevent direct contact between the copper plates.

The as-received material was not conductive; however, after treatment the particles exhibited very low resistance. The oxide should not be present according to the manufacturer specifications, and repeated inquiries to the vendor were not returned. Perhaps most telling is that the vendor has since pulled this product from the market. This is unfortunately a widespread issue when working with sub-micron or nano fillers.

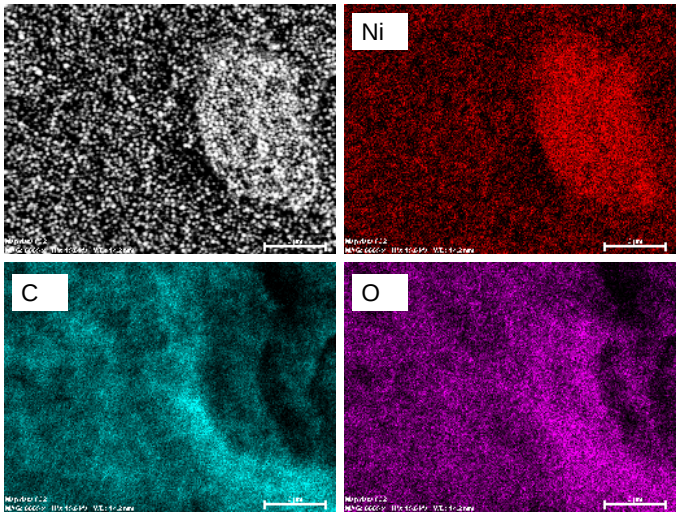


**Figure 15. EDS mapping of nickel, carbon and oxygen signals revealing presence of probable oxide layer.**

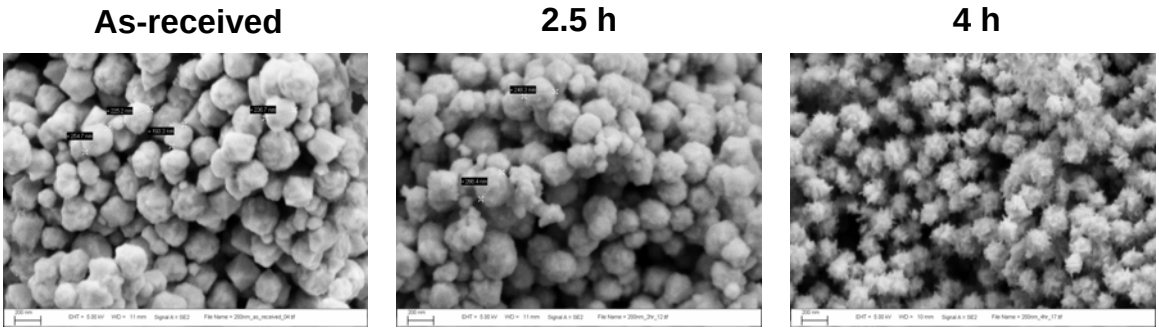


**Figure 16. SEM images of HCl treatment of 200 nm nickel particles as a function of exposure time.**

## 3.4 Impact of Particle Loading

### *3.4.1 Difference in Processing Limitations*

Although the presence of an oxide layer explains the lack of conductivity, it does not explain the difference in processing limitations. The 2-4 μm nickel particles could only be processed to 30 volume % where as the 200 nm particles could be loaded to 40 volume %. This is in contrast to what is typical in suspensions with the continuous phase less viscous than the polymer used here, where colloidal effects can increase the apparent viscosity of the mixture as the particle size is decreased below about 1 μm. To help determine if this observed difference in processability is inherent to the particles or an artifact of the processing conditions, 30 volume % of both fillers was added to a low viscosity Epon 828 resin (Figure 17). The 200 nm filler was easily mixed into the resin and was completely wetted. In contrast, the 2-4 μm was not completely wetted by the resin. This same behavior was also observed in aluminum oxide particulates where faceted particulates exhibited a significantly higher impact on the viscosity than uniformly shaped particles. Thus, this behavior is attributed to the irregular shape of the micron sized particulate. More uniformly shaped 10 μm nickel spheres were ordered from Incospec but did not arrive in time to be incorporated significantly into the study.

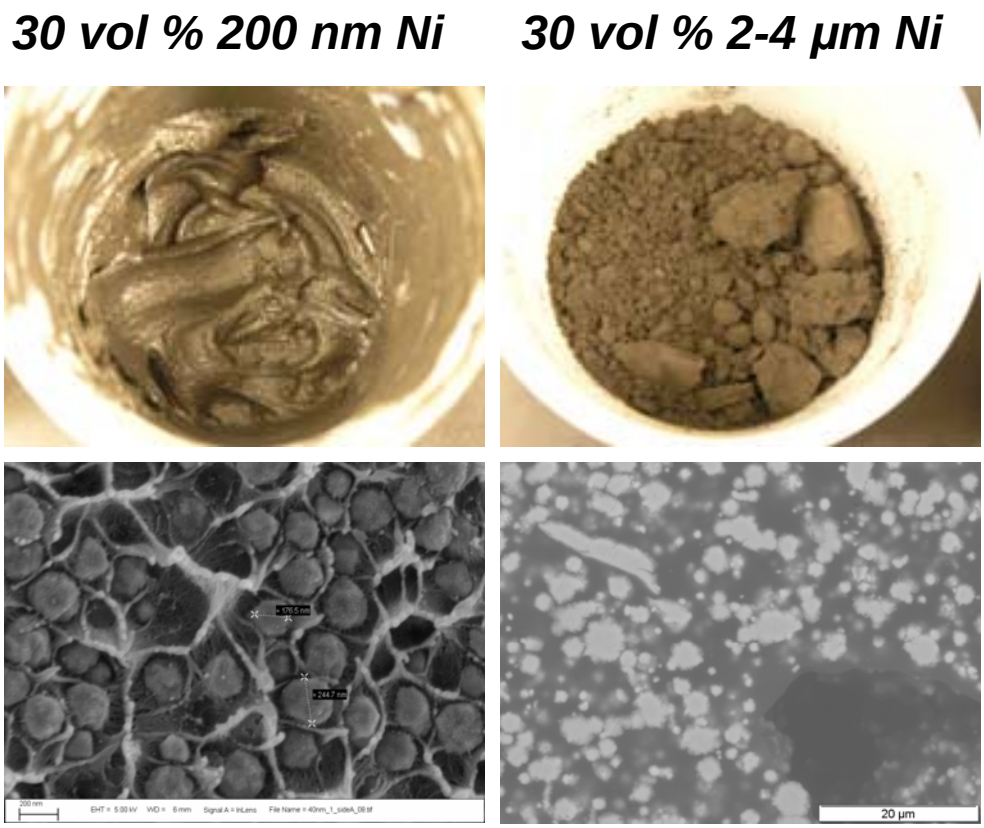


**Figure 17. Pictures of Epon 828 with 30 vol % of 200 nm and 2-4 µm nickel particles along with SEM images demonstrating the difference in shape.**

### *3.4.2 Quantifying the Impact of Particle Loading*

Parallel plate oscillatory rheometry was used to quantify the impact of the type and amount of added particles on the apparent dynamic moduli of the mixtures. A well-known empiricism (the Cox-Merz rule) states that the linear dynamic viscosity η* versus frequency curve is virtually identical to the steady shear viscosity η versus shear rate curve [Renardy 1997, Gleissle & Hochstein 2003]. It is easy to get dynamic data over a wide range of frequencies; whereas steady shear measurements over a similar range of shear rates usually requires more than one type of instrument. However, the Cox-Merz rule is not reliable when used with suspensions, although Gleissle & Hochstein showed that, with appropriate corrections, η* can be

related to η as long as the oscillatory measurements are conducted within the linear viscoelastic range [Gleissle & Hochstein 2003].

The dynamic viscosity was determined at 1 % strain using a frequency range of 0.01 to 300 radians/s (Figure 18). As expected, the viscosity increased as the particle loading was increased. In addition, there was a distinct decrease in the measured viscosity with increasing frequency referred to as shear thinning. (It may be possible to use the considerable frequency dependence and shear thinning behavior to minimize the mismatch between the layered materials by extruding at higher shear rates.) This also resulted in the reduced viscosity as function of loading being very dependent on the frequency at which it was measured. It is clear that even at relatively modest rates, 40 volume % 200 nm nickel loading had a considerable impact on the viscosity of the material.

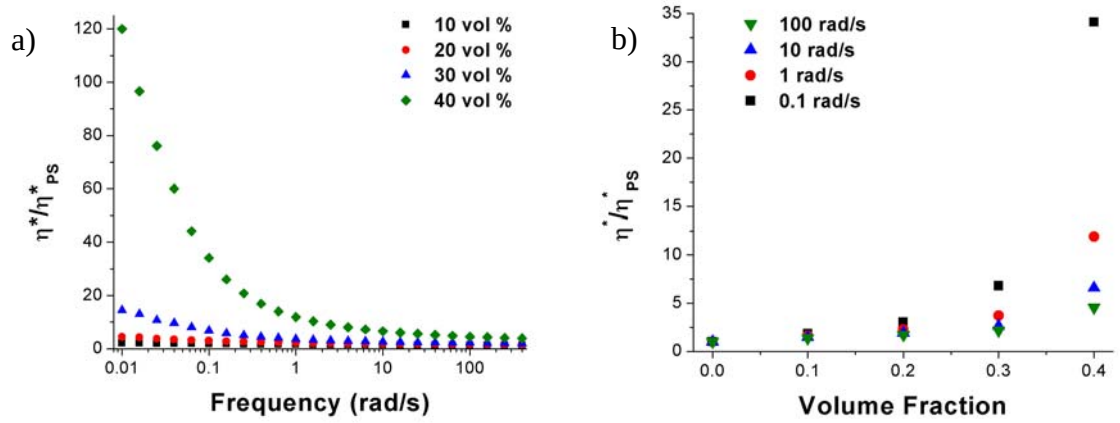


**Figure 18 a) Reduced viscosity as a function of frequency for various loading of 200 nm nickel particles. b) Reduced viscosity as a function of loading at various frequencies.**

Quantifying the impact of the micron sized nickel loading proved far more difficult. Prior to measuring the frequency dependent dynamic viscosity, a strain sweep was performed to ensure that the test was run in the linear regime. Strain sweeps of polystyrene loaded with 30

volume % micron nickel at 3 different frequencies were not linear (Figure 19a). As a result the measured values were very dependent on not only the frequency but the strain that was chosen, and as mentioned above the Cox-Merz rule would not apply. Therefore, the values will only have meaning in a very limited range of parameters. For comparison, the strain sweeps of the pure polystyrene matrix exhibited a non-linear regime at low strains and then became independent of strain rate (Figure 19b). This did not appear to be due to the presence of particulate in general as the 40 volume % 200 nm had a large linear region. The large non-linear region was likely due to the non-uniform shape and faceted nature of the filler, which made the maximum packing of the particles lower. As low as at 30 volume % solids, the particles were near the jamming limit, and noticeable air bubbles formed in the sample during testing. Degassing in a vacuum oven and repeated testing to remove initial air bubbles were unable to decrease this behavior. The issues present in oscillatory testing of the suspension led us to use steady shear rheology in future tests, as will be described in Section 5.

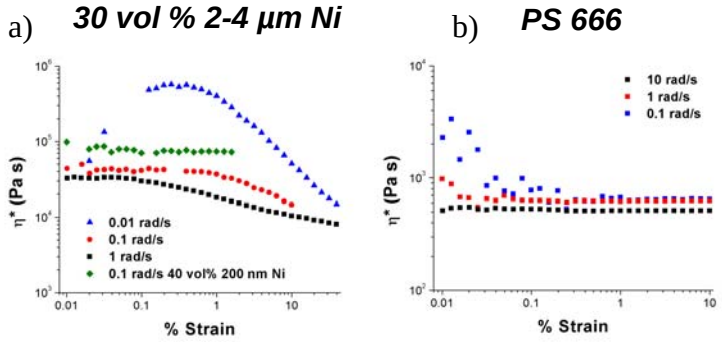


**Figure 19. a) Strain sweeps of a composite of polystyrene and 30 volume % of the micron-sized nickel in a parallel plate geometry at three different frequencies, along with a 40 volume % 200 nm nickel strain sweep in green for comparison. b) Strain sweeps of the polystyrene matrix at three different frequencies.**

## 3.5 Incorporation of a Low Melting Eutectic Metal

To produce a highly conductive melt processable material the incorporation of a low melting eutectic metal was explored. The concept is that the low melting filler will be molten during processing to reduce the impact on the viscosity but will be solid at the anticipated operational temperature of the device. To test this concept we used a eutectic metal mixed with the nickel – polystyrene materials described earlier. The eutectic material used consisted of 58 % bismuth and 42 % tin, a commercial material called Cerrotru (McMaster-Carr). The material melts at 138 ºC well below the extrusion temperature of approximately 260 ºC. Bismuth is unique in that it expands when cooled. As a result, the material has a very low net expansion of 0.05 % when changing from a solid to a liquid. This should reduce any internal post extrusion strain. Finally, the eutectic has already been explored as a lead-free solder replacement for use with nickel electrodes [Tao et al. 2001]. As a result, the electrical and mechanical contacts with nickel have been previously established.

## 3.6 Impact of the Eutectic on Composites using Micron Particles

The addition of nickel was critical to dispersing large quantities of the eutectic metal. In the absence of nickel, the eutectic was initially dispersed but during processing dispersed eutectic droplets will coalesce and phase-separate out of the material leaving ~ 2 volume % eutectic metal well dispersed (Figure 20). While the mechanism of the co-operative interaction is still unclear, it is likely that the nickel particulate acts as a mixing aid to further break up the liquid droplets and/or acts as a stabilizing surface to inhibit phase separation. SEM images of the composite samples indicated that the filler microstructure was initially uniformly dispersed nickel particulate along with larger areas of brightly colored eutectic intermittently dispersed throughout the sample (Figure 21). As the eutectic loading was increased to 40 volume %, the concentration of the droplets increased while the relative size of the eutectic droplets decreased.

When the eutectic loading was increased to 50 volume % the microstructure changed from relatively small droplets on the order of 10 μm towards a microstructure where the individual droplets appear to coalesce together. Cross-sectional images were taken both parallel and perpendicular to the extrusion direction and were not noticeably different indicating the extrusion did not produce any anisotropy (Figure 22).

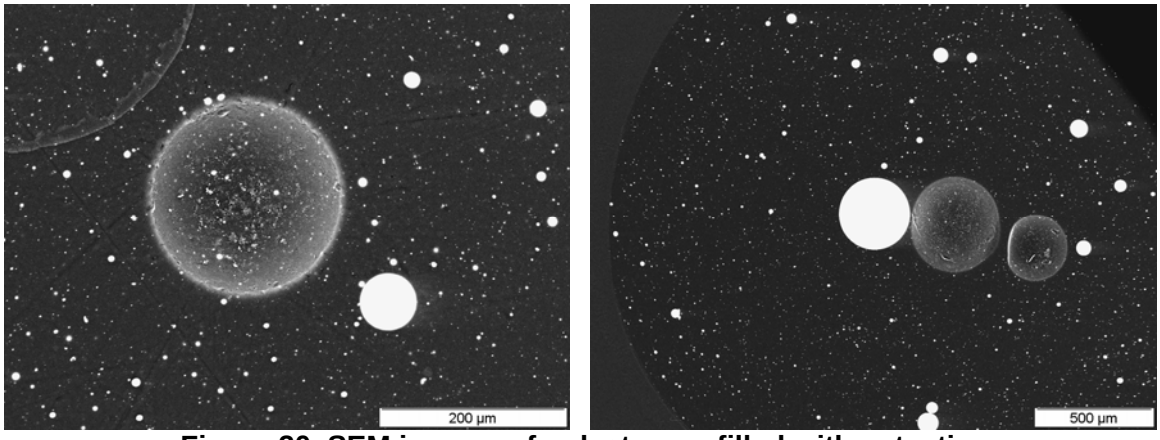


**Figure 20. SEM images of polystyrene filled with eutectic.**

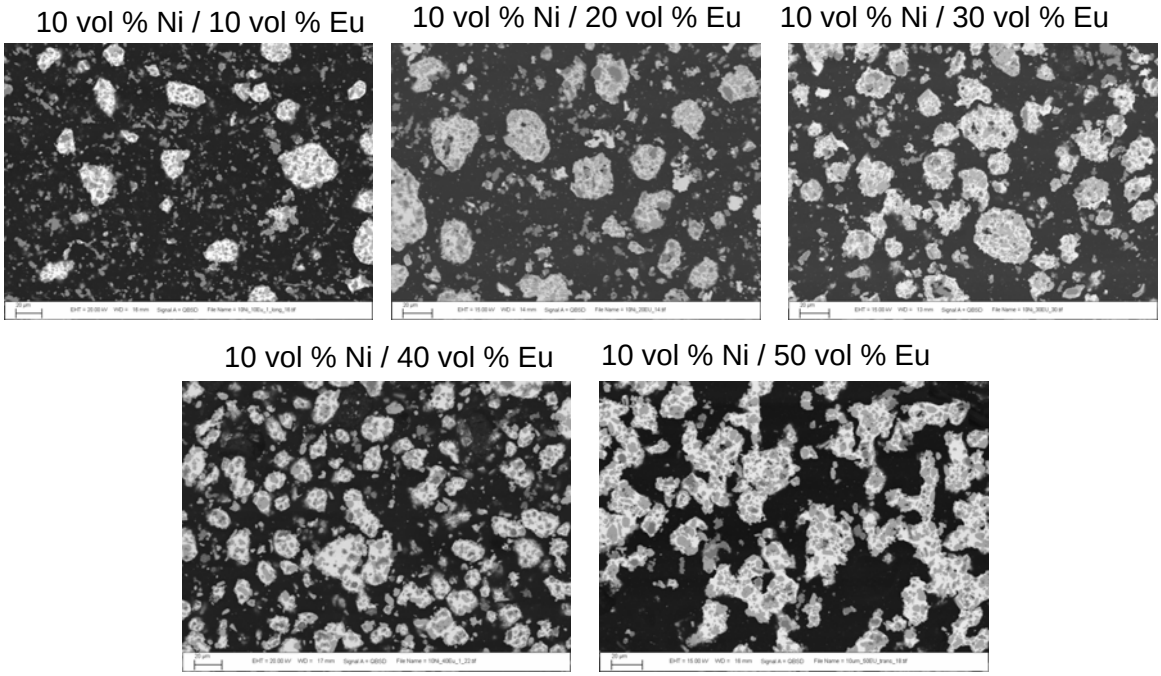


**Figure 21. SEM images of the composite microstructure as the loading of eutectic was increased while maintaining 10 volume % nickel loading.**

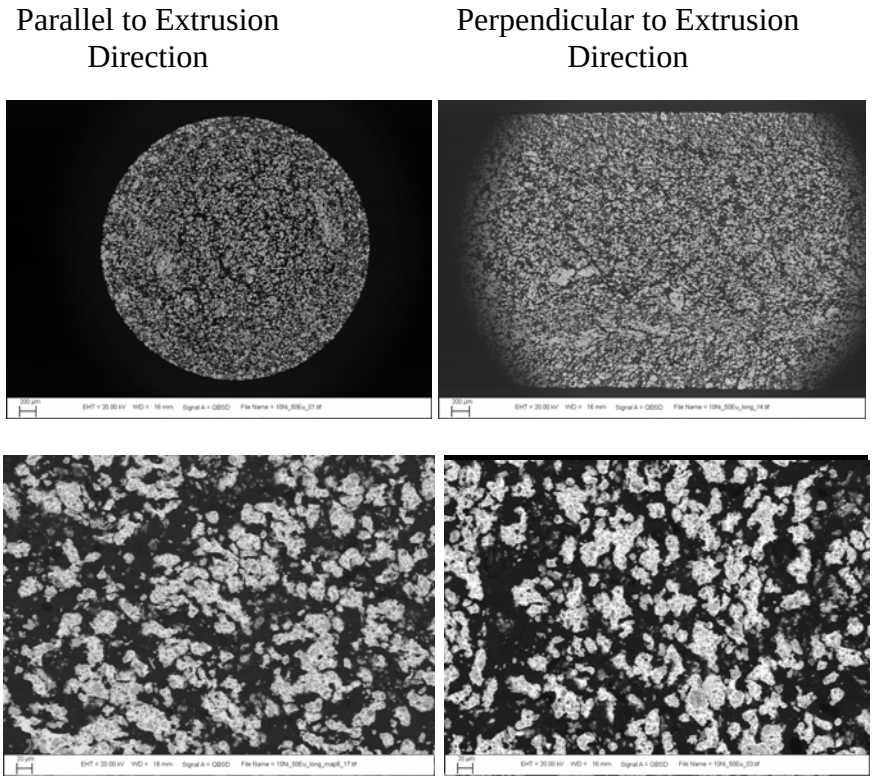


**Figure 22. SEM images of polystyrene containing 10 volume % nickel and 50 volume % eutectic both parallel and perpendicular to the extrusion direction.**

To gain additional insight into the co-operative interaction of the nickel particulate and eutectic metal, constituent elements were mapped in the SEM using EDS. Figure 23 contains the bismuth, tin, and nickel maps obtained from EDS for a sample containing 10 volume % nickel and 50 volume % eutectic. From these images, it appeared that there was a high concentration of nickel in the areas where there was eutectic but outside of those areas there was very little nickel. Inside the metal rich regions, the nickel and tin signals overlapped and were surrounded by the bismuth. This indicated that during phase separation, typical of eutectic materials, the tin was nucleating on the nickel. Whether this indicated that the tin had some affinity for the nickel or whether the nickel just provided a solid surface to facilitate nucleation was unclear. Previous work investigating this eutectic as a lead-free solder for use with nickel electrodes demonstrated that a $Ni_3Sn_4$ interfacial alloy will form. The strong interaction of the filler had a pronounced impact on the microstructure. At low eutectic loadings there was a large amount of nickel outside the eutectic droplets; however, as the loading increased the amount of nickel present outside of the eutectic droplets was considerably decreased. This microstructural change was verified by mapping the tin and nickel samples using EDS (Figure 24). In these images, the nickel signal decreased as the eutectic loading increased despite the fact that the nickel loading remained the same.

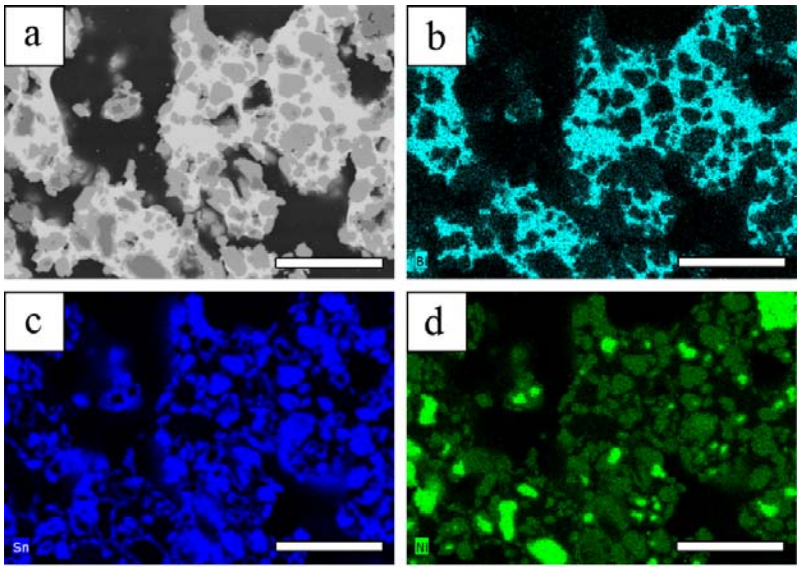


**Figure 23. a) SEM image of polystyrene containing 10 volume % nickel / 50 volume % eutectic along with EDS maps of b) bismuth, c) tin, and d) nickel. Scale bars are 50 um long.**

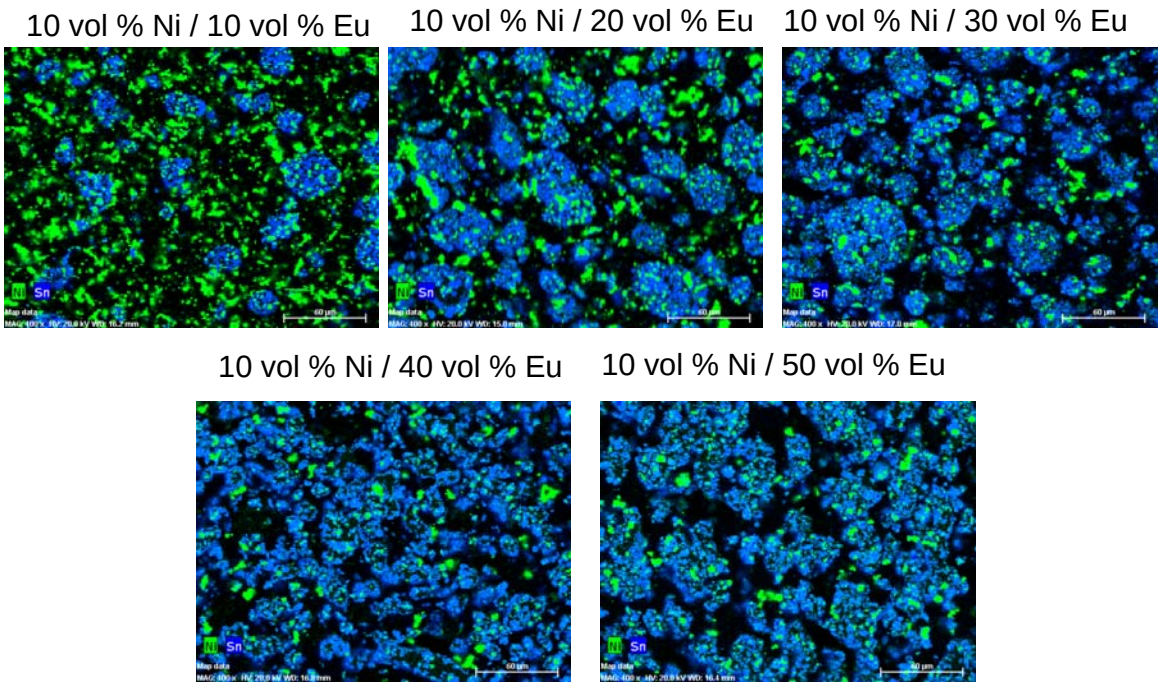


**Figure 24. EDS mapping of the tin and nickel sample of polystyrene with increasing eutectic loading while the nickel loading was maintained at 10 volume %. Nickel is indictated in green and tin in blue.**

## 3.7 Impact of Eutectic Addition on Composites using Sub-micron Particles

In contrast to the eutectic behavior in the presence of the micron sized particulate, the eutectic was not easily incorporated into the polystyrene with the smaller nickel particles. The eutectic droplets coalesced as they did when dispersed without nickel at all. At even low eutectic loadings the droplets would phase separate out of the composite. This behavior was supported by the SEM images that exhibited areas of light gray consistent with nickel and distinct, mostly circular, brightly colored regions consistent with the eutectic (Figure 25). In addition, the eutectic had very little impact on the observed processability of the composite during extrusion. The SEMs showed air voids and an irregular cross-section that is attributed to an increase in viscosity. The lack of co-operative mixing was verified using EDS to map the constituent elements (Figure 26). In these images the nickel signal was present in most of the area except in the area of the eutectic droplet.

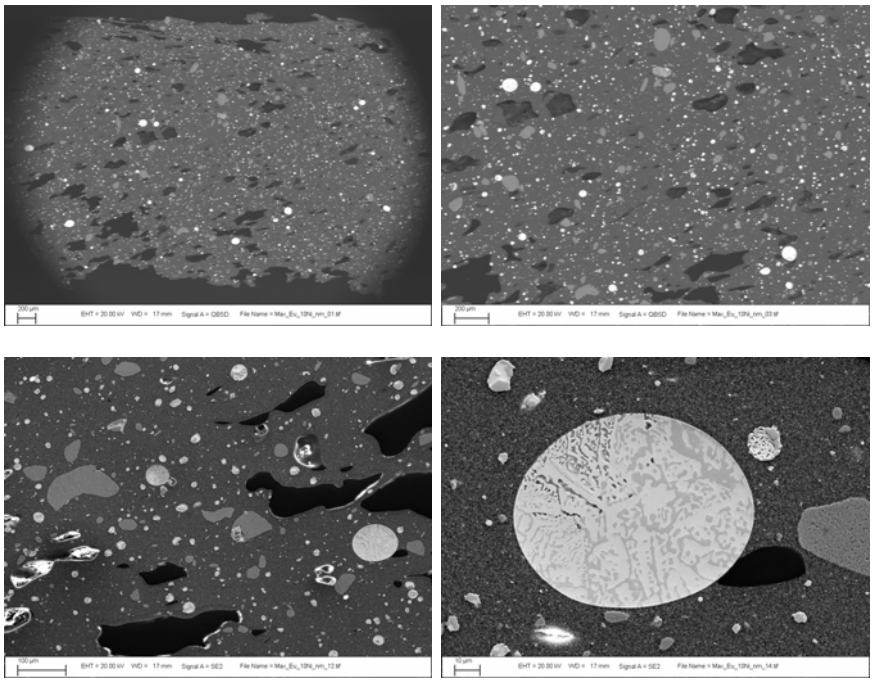

**Figure 25. SEM images of polystyrene with 10 vol % 200 nm particles and eutectic.**

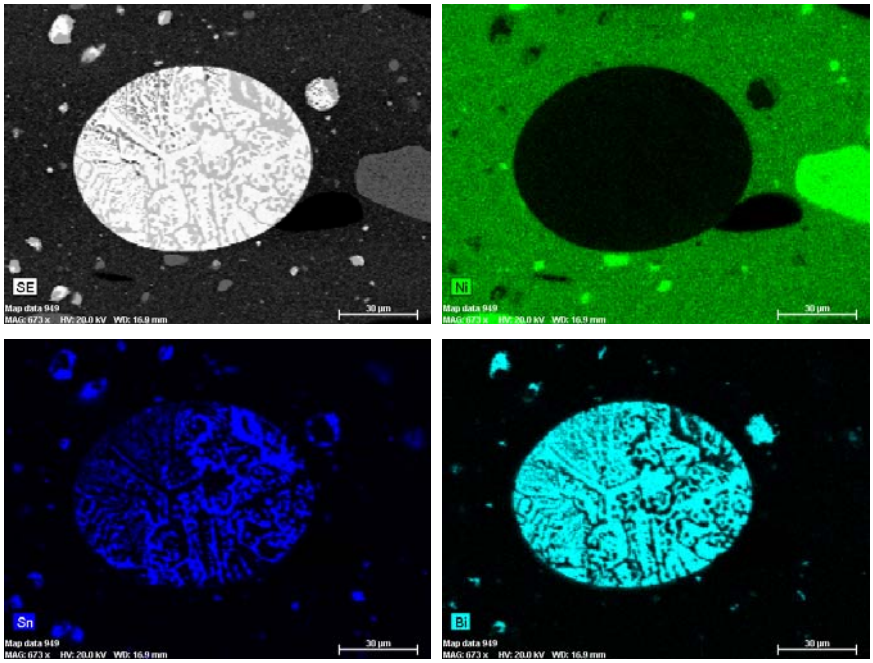


**Figure 26. EDS maps of polystyrene with 10 volume % 200 nm particles and eutectic.**

It is possible that the presence of an oxide layer on the 200 nm nickel particles led to a change in the eutectic dispersion. To test this hypothesis 200 nm nickel particles were treated with hydrochloric acid to remove the oxide coating. Mixing the eutectic along with the acid treated 200 nm nickel initially incorporated more eutectic but eventually exhibited phase separation at only modest loadings. SEM images of the sample indicate that the eutectic and treated 200 nm nickel were somewhat better dispersed (Figure 27) than when untreated particles were used. The texture of the eutectic droplets changed from the untreated particles indicating that nickel was present. The presence of nickel was verified using EDS (Figure 28). While the nickel was present inside the eutectic droplets it did not appear to be well dispersed. This may have been a result of the surface treatment procedure not being able to penetrate the aggregates. Perhaps improving the dispersion during the acid treatment would produce a composite that would be able to incorporate more eutectic.

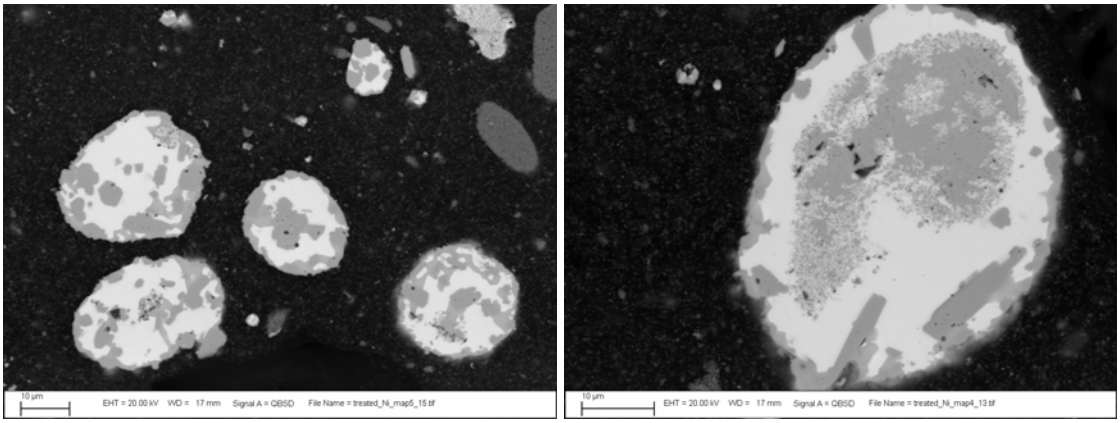

**Figure 27. SEM images of polystyrene with surface treated 200 nm particles along with eutectic metal.**

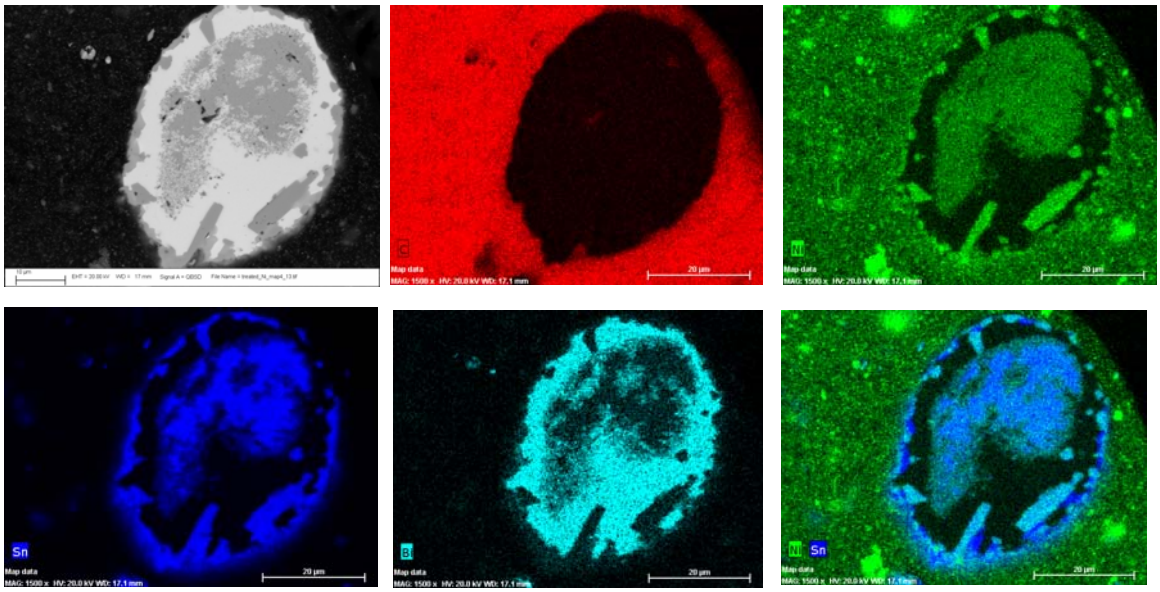

**Figure 28. EDS maps of polystyrene with surface treated 200 nm particles along with eutectic metal. The color coding is as follows: Red is carbon, green is nickel, blue is tin, turquoise is bismuth.**

## 3.8 Impact of Eutectic Addition to the Conductivity of Composites using the Micron-sized Particles

The eutectic metal was added in 10 volume % increments to a mix of polystyrene and nickel, keeping the nickel content constant at 10 volume %. The composite resistance of the extruded material was measured using a Signatone S-302-4 four point resistivity probe attached to a

Keithley 2410 source meter. To qualitatively determine the macroscale conductivity, the four point probe measurements were compared to resistance values obtained by attaching leads across lengths ($L$) of extruded material from 20 – 65 cm. Figure 29 shows example cross-sections of the extruded pieces. One side of the cylindrical extruded sample was sanded so that the sample would lie flat. The probe yields sheet resistivity directly in ohm/square, traceable to a NIST standard. However, note that the probe configuration is assumed to be measuring a sheet of width $W$ and length $L$, where the sheet thickness $t$ is less than the diameter of our extrudate. Nevertheless, it is reasonable to compare relative values. It is also interesting to note that when the probes were attached to the sanded side, the results did not vary significantly.

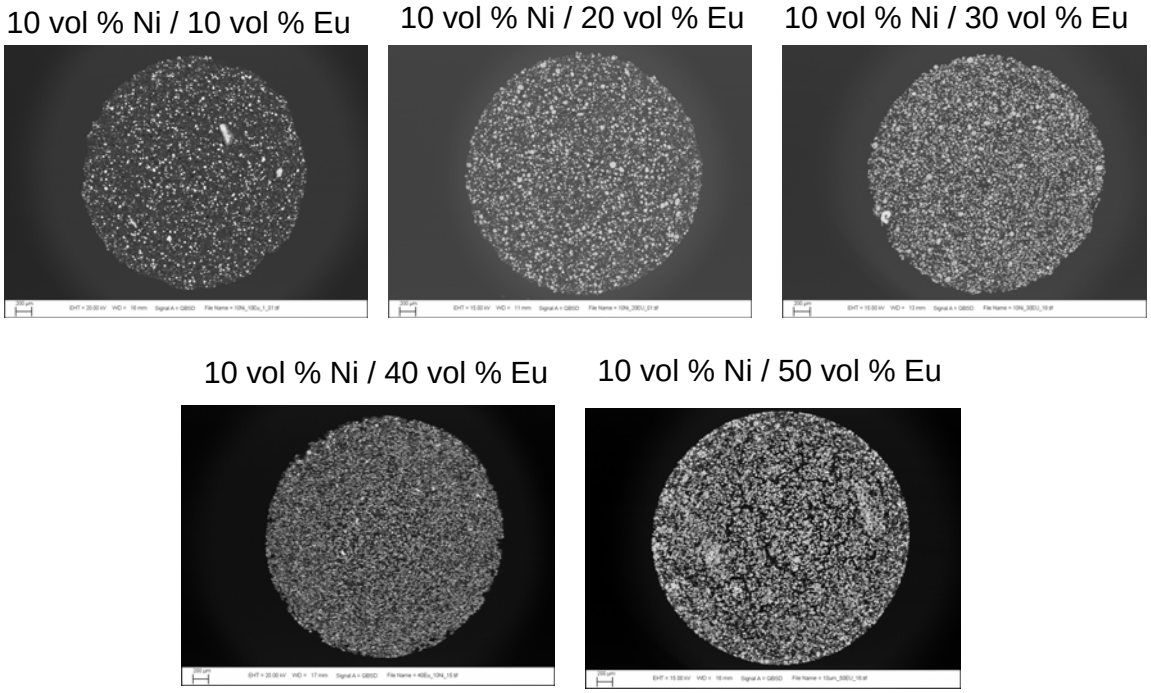


**Figure 29. SEM images of the extruded material cross-section perpendicular to the flow direction.**

The composite exhibited a measurable sheet conductivity at 30 volume % metals loading (10 volume % nickel / 20 volume % eutectic) of ~ $2 \times 10^{-6}$ Siemen-square (S-sq), where 1S=1/Ohm

and a square is the dimensionless L/W of the sheet (Figure 30). At 40 volume % metals loading the conductivity increased to ~ 1 S-sq and then approached 10 S-sq at loadings of 50 and 60 volume % metals loading. In addition, the composites were conductive over large distances. For example, a 65 cm strand with 50 volume % metals exhibited an end-to-end resistance of less than 1.3 Ω (Figure 31). To put this in perspective, the 2-4 μm nickel particles mixed into the polystyrene alone exhibited a measurable conductivity of $2 \times 10^{-4}$ S-sq at 20 volume %.

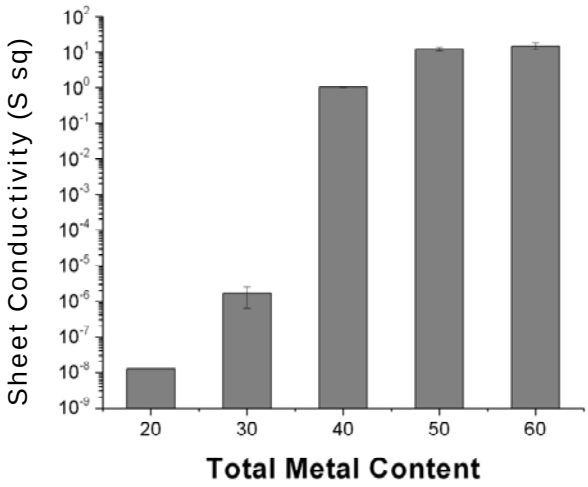


**Figure 30. Sheet conductivity of polystyrene filled with increasing eutectic loading while maintaining a constant nickel loading of 10 volume %. Values are reported as the total metal content.**

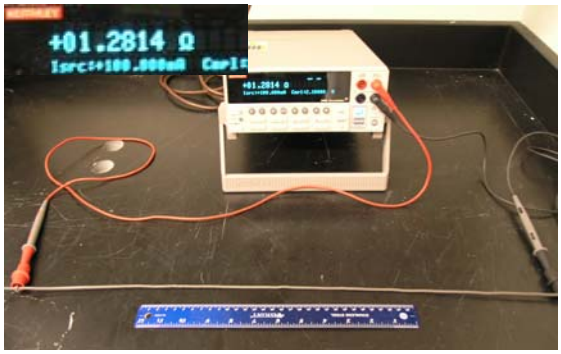


**Figure 31. Photograph of a composite with a total metal content of 50 volume % attached to a Keithley 2410 sourcemeter with the test leads 65 cm apart. The inset is a larger view of the sourcemeter readout.**

The results can also be interpreted as a bulk conductivity ($\sigma$) which is equivalent to 1 divided by the bulk resistivity ($\rho_r$), both material properties independent of the geometry. However, this assumes that the material is homogeneous throughout the volume, which in a multiphase system is not necessarily true. These properties are related to the measured resistance ($R$) in Ohm/cm by:

$$\sigma = 1/\rho_r = L/RA = L/R(\pi r^2), \qquad \textbf{5}$$

where $r$ is the radius of the extruded piece of material. Conductivity is in units of S/cm. This is a way of comparing data taken by simply measuring the resistance between two alligator clips, as had been done with the material loaded with nickel particles only, and a way of comparing data on samples of different diameter. The conductivity $\sigma$ and the measured conductance ($1/R$) of the nickel/eutectic samples are shown in Figure 32 and 33, respectively. Effects of decreasing the amount of nickel, while keeping the amount of eutectic high (the last column in these figures) are discussed in the next subsection.

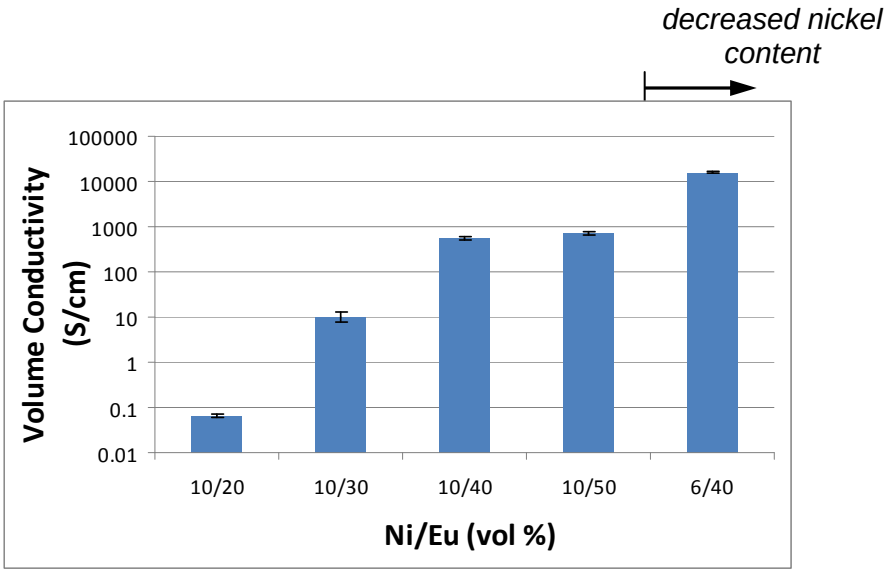


**Figure 32. Conductivity values for composites with varying nickel and eutectic loadings corrected for geometry.**

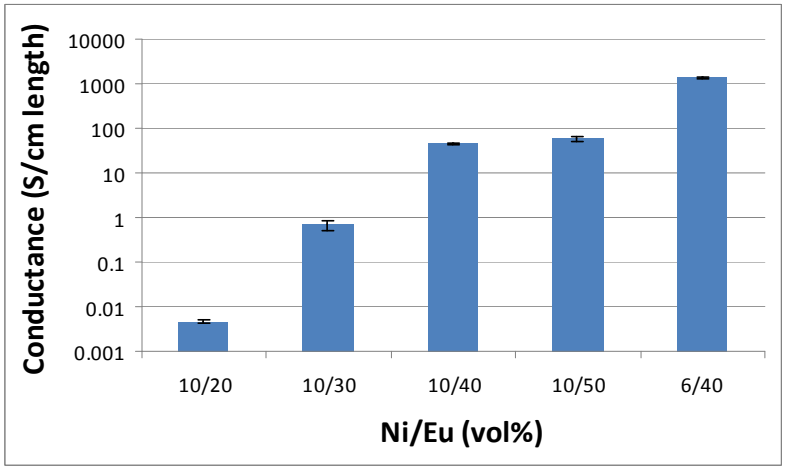


**Figure 33. Conductance measured per unit length of extruded "wire".**

## 3.9 The Effects of Increasing the Ratio of Eutectic to Nickel Particles

To explore composites with lower nickel content, we made a sample consisting of 6 volume % nickel and 40 volume % eutectic. All of the eutectic was easily dispersed without the eutectic phase separating from the material. In an attempt to determine the limits of processing

and enhance the mixing, we extruded the sample as fast as the extruder could operate. As a result the material started to have an irregular surface texture but was extruded without a problem. SEMs of the collected material revealed a very distinct microstructure change (Figure 34). The eutectic was no longer uniformly dispersed and appeared to have formed large elongated droplets. Images parallel and perpendicular to the sample revealed that the droplets were oriented closer to the wall, but that this orientation did not extend into the center of the extruded material. The electrical properties of the material were very good measured in the direction of extrusion. A 1 meter piece of material was extruded with an end-to-end resistance of 0.7 Ω (7 × 10-4 Ω/cm length). As a result, a higher conductivity was obtained at a lower overall metal content presumably due to processing conditions (Figure 32). Unfortunately, the conductivity in the direction perpendicular to extrusion is more important in the case of co-extruded capacitors. Nevertheless, this behavior could be useful in other applications. More results of the effect of the mixture morphology are discussed in the next section.

Parallel to Extrusion Direction

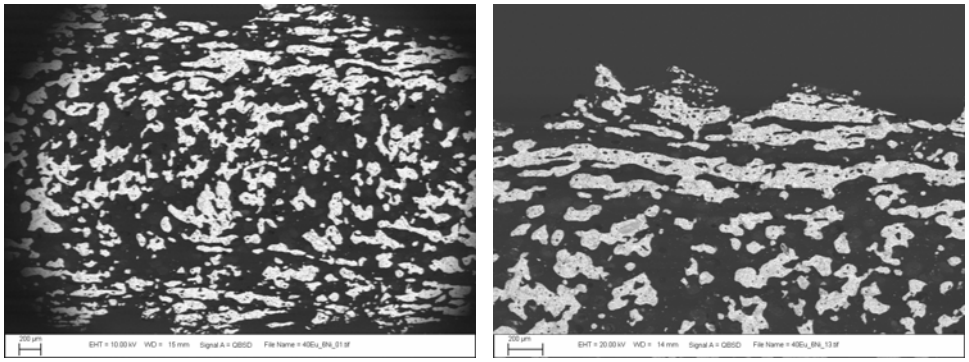

Perpendicular to Extrusion Direction

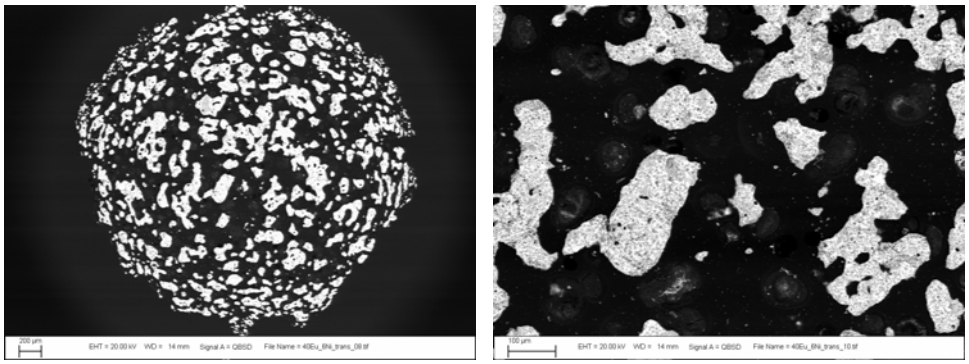

**Figure 34. SEM images of a polystyrene composite containing 6 vol % nickel and 40 vol % eutectic both parallel and perpendicular to the extrusion direction.**

## 3.10 Processing Studies Using Twin-Screw Extruders: Minilab

Processing large amounts of material with the single screw extruder was time consuming. We were lucky to acquire the use of two twin-screw extruders, although this was late in the project. The first, a Haake Minilab (Thermo Scientific), includes recirculation for higher residence time and better mixing (Figure 35). The main disadvantage of this equipment was the small volumes of material that could be mixed. The second disadvantage was that phase segregation could be significant, as will be discussed in the next paragraph.

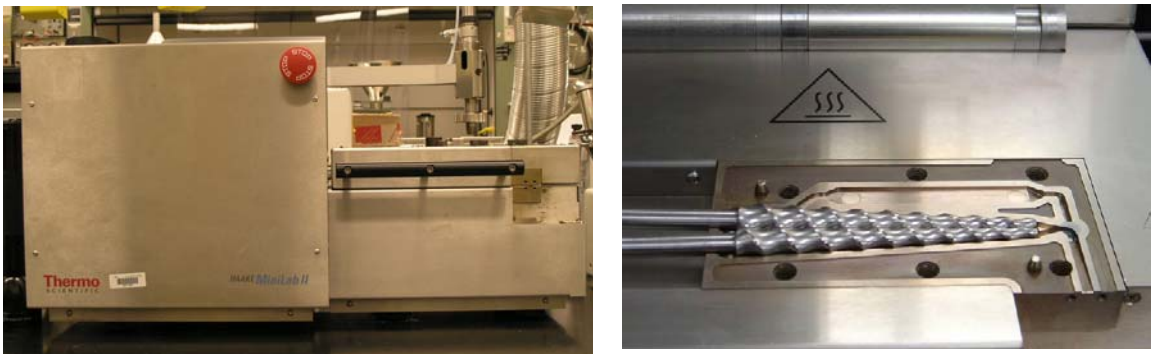


**Figure 35. Photos of the benchtop Haake Minilab. Right, interior showing recirculation channel.**

More 2-4 μm nickel-eutectic-polystyrene composites were tested using this extruder in order to assess the effects of the degree of mixing and to explore more thoroughly the relationship between conductivity and formulation. All tests were performed at 240ºC. One noticeable problem with processing any formulation containing the eutectic in the Haake Minilab was that eutectic tended to separate from the mix and get trapped in a region in the back of the screws. It could often be seen floating on the top of the rest of the material before finally being incorporated. Therefore, it was difficult to add eutectic to high loadings relative to the nickel. On the other hand the barrel could plug when the nickel loading was as little at 15 volume%. All samples were tested with TGA to make sure that the metals loading of each was actually that introduced into the mixer.

The conductivity of samples of various compositions were tested (Figure 36), and the results were not as clear cut as the earlier tests of materials processed with the single screw extruder. Each batch of material was approximately 50g or 7 ml, and each sample tested was approximately the same diameter (that of the cooled extrudate) and of a length equal to 15.2 cm. In general the conductivity of the material increased as the total metals loading increased, but no

clear advantage of an increase in the relative amount of eutectic was observed. Not always, but frequently the conductivities of samples mixed in the twin-screw extruder were less than similar compositions created in the single screw extruder. We speculated that mixing was an important parameter and that the degree of mixing had a large influence on the results.

Unfortunately, it appeared that, at a fixed metals loading, the better the mixing, the higher the resistance. This variation is thought to be the most likely cause of the large scatter in the data. For example, in Figure 36, the points for the 10% nickel and 40% eutectic in polystyrene, for a total metals volume % of 50, show a dramatic increase in resistance when the initial batch is remixed. This seemed to be confirmed by SEMs taken of the highly conductive material extruded in the single screw extruder (reported in Figure 32) compared to less conductive material with the same composition. Figure 37 shows SEM of these two materials. In material that included the eutectic, the material that seemed to display the lowest resistance also showed signs of separated eutectic on the surface. When pressed into a thin disc, the material with the lowest resistance showed distinct separation of the eutectic material, in contrast to the better mixed material (Figure 38). The lowering of the conductivity by better mixing is attributable to better coating of the conductive material with polymer, hence isolating the particles/droplets from each other and hindering the formation of a percolated network. Similar results have been discussed in the literature (Kalyon et al. 2002).

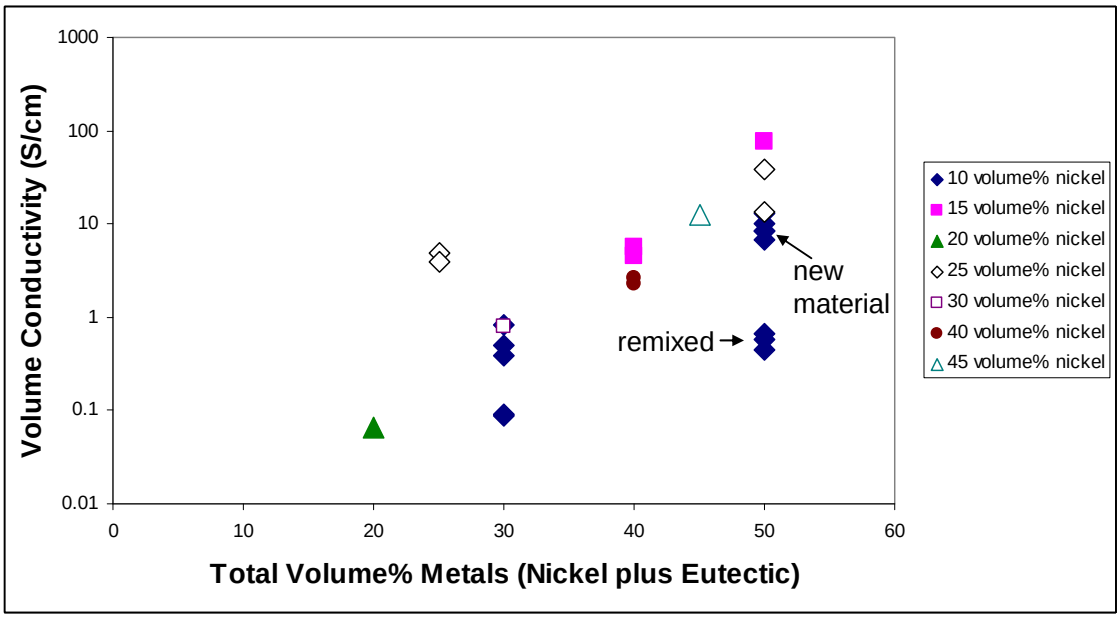


**Figure 36. Conductivity of 15-cm lengths of extrudate from the Haake minilab. Various compositions are shown, where the volume % of the eutectic is the total volume % of metal (the abscissa) less the amount of nickel shown in the legend.**

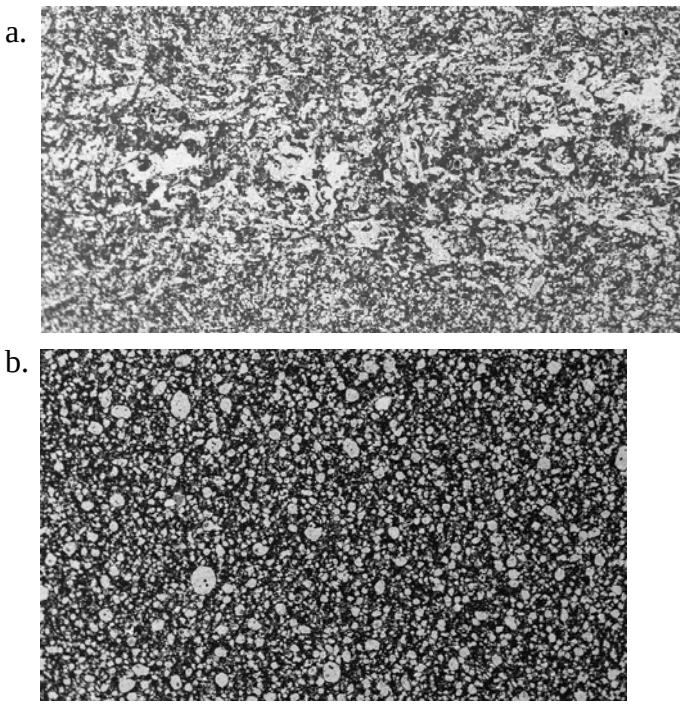


**Figure 37. SEMs of material with 46 volume % polystyrene, 40 volume % eutectic, and 6% nickel 2-4 μm particles with very good conductivity (a) and that is less conductive (b).**

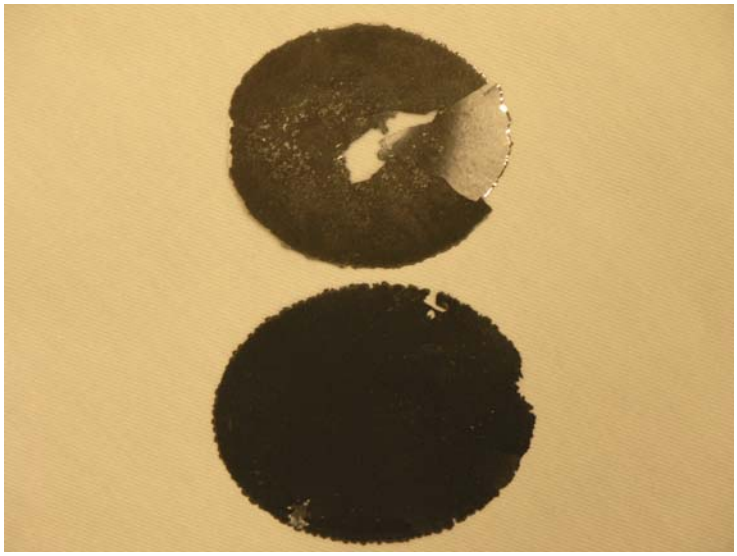

**Figure 38. Top sample showed very low resistance but phase separated when pressed flat.**

## 3.11 Potential Capacitance

Samples of several materials were tested as the conductive material in a simple capacitor. Here each composite material was pressed into a disc 0.157 cm thick, then placed in a stack with a copper plate on the bottom, followed by a Kapton sheet in the middle, then the composite on the top. Capacitance ***C*** was measured using a four-wire bridge. Theoretically,

$$C\ (pF) = K*Eo*A/D, \qquad 6$$

and:

***K*** is the dielectric constant of the Kapton,

***A*** is the overlapping surface area of the plates ($cm^2$),

***D*** is the distance between the plates (cm), and

***Eo***$= 2.2489 \times 10^{-11}$ (pF/cm)

The ratio of the measured capacitance to the calculated theoretical values (equation 6) correlated with the amount of conductive material distributed within the polymer, consistently. For example, for a sample with a total metals loading of 50 volume %, the calculated theoretical

value was 61.9 pF, but the measured value was 31 pF. Another sample with 40 volume % total metals loading had a theoretical capacitance of 49 pF, but a measured value of 20 pF. Another sample with 10 volume % nickel (and no eutectic), when joined with a layer of Mylar, had a theoretical capacitance of 980 pF, but a measured value of 98 pF. We believe that the reduced capacitance is the result of the actual ***A*** not being that of the total surface, but reduced to only that of the conductive material in that surface.

## 3.12 Processing Studies Using Twin-Screw Extruders: Large Extruder - Effect of Flow Rate and Temperature

After testing candidate materials in the Minilab, we switched to a large extruder, a Haake Rheomex OS PTW16 twin screw mixer driven with a PolyLab OS Rheodrive 7 drive unit (Thermo Scientific), to make batches of a reasonable size for testing in the co-extruder (Figure 39). This instrument has multiple heating zones and can process much more material than the smaller Minilab in the same amount of time. However, the material does not recirculate and must be taken from the extruder exit, pelletized, and returned to the inlet in order to better mix the final product.

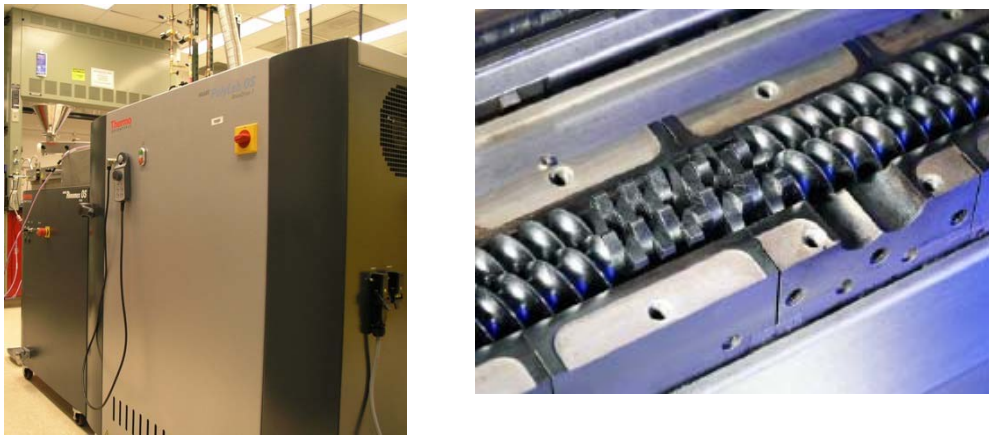

**Figure 39. Photos of the large free-standing Haake twin screw extruder. Right, interior.**

We decided that we would compromise between the needs for processability and conductivity and produce a composite with 40 volume % total metals, with a composition of 12 volume % 2-4 μm nickel particles and 28 volume % eutectic. With this formulation we tested several temperatures and screw speeds to see the effects on the final product. The test matrix is shown in Table 1. The data was taken after a gradual addition of the metals to the polystyrene. The final mixture was pelletized after extrusion and remixed once more in the large extruder. The material in Test 1A and B had much higher resistance than the material in the other tests. We speculated that this was because the extruder started dry, and the first material out included excessive air pockets. Once the extruder had been run for a time, the material seemed more consistent, so Tests 1A and B were not included in the following studies, but the same conditions were repeated at the end. Again, this emphasizes the difficulties in mixing these multiphase materials. After the extrusion had stabilized at an exit temperature of 225ºC, the extruder (full of material) was stopped, and the temperatures of the downstream zones were increased. When the temperatures stabilized, the machine was restarted and the material flushed with new material before samples were taken. Photos of the extrudate show that the material thinned and the surface became rougher as the temperature increased (Figure 40). No significant visual difference was observed with increasing screw speed (Figure 41).

**Table 1. Screw Speed and Temperatures for Large Twin-Screw Extruder Tests**

| Test # | RPM | Zone 1 | Zone 2 | Zone 3 | Zone 4 | Zone 5 | Zone 6 | Zone 7 | Zone 8 | Zone 9 | Zone 10 |
|---|---|---|---|---|---|---|---|---|---|---|---|
| 1A | 7.5 | 195 | 210 | 225 | 225 | 225 | 225 | 225 | 225 | 225 | 225 |
| 1B | 15 | | | | | | | | | | |
| 2A | 7.5 | 195 | 210 | 225 | 225 | 230 | 230 | 235 | 235 | 240 | 240 |
| 2B | 15 | | | | | | | | | | |
| 3A | 7.5 | 195 | 210 | 230 | 235 | 240 | 245 | 250 | 250 | 260 | 260 |
| 3B | 15 | | | | | | | | | | |
| 4A | 7.5 | 195 | 210 | 225 | 225 | 225 | 225 | 225 | 225 | 225 | 225 |
| 4B | 15 | | | | | | | | | | |

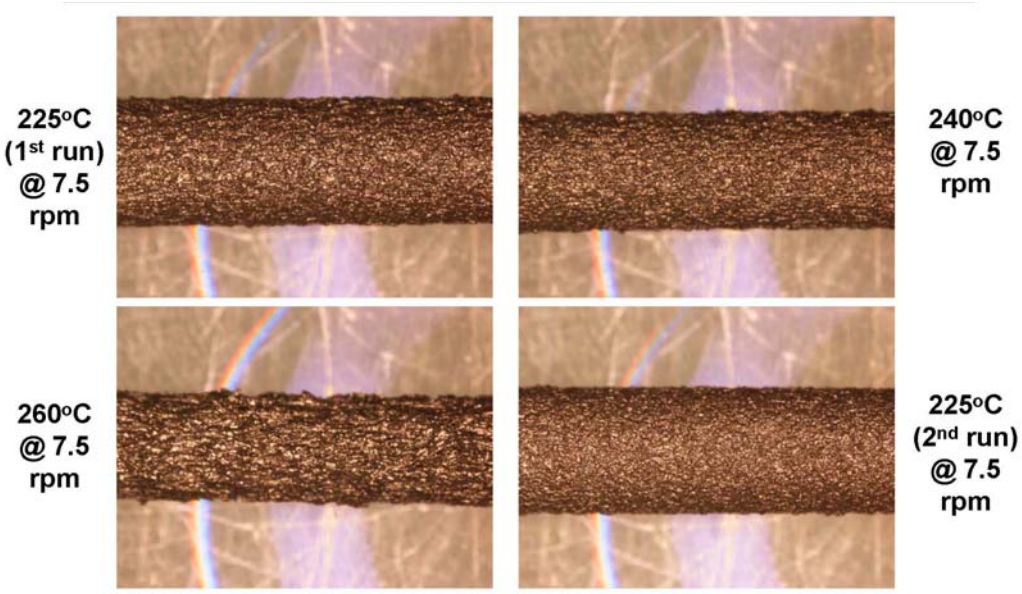


**Figure 40. Large twin-screw extruder results show that the extrudate thins and becomes rougher at higher temperatures. The first run at 225ºC was somewhat rougher than the second run and exhibited unusually high resistance. We believe that the extrudate had not stabilized sufficiently and may have included more air.**

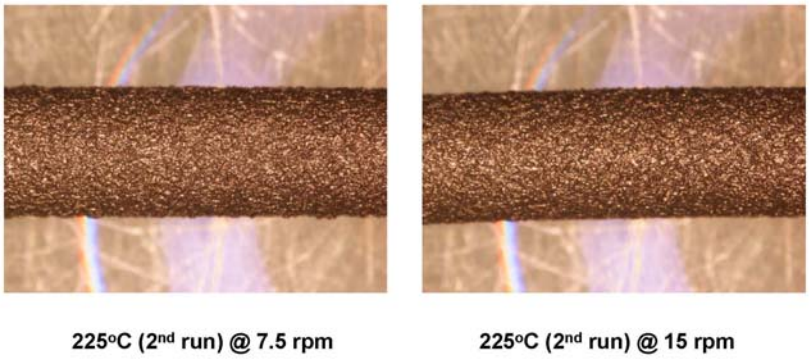


**Figure 41. No significant visual difference was detected in changing the speed from 7.5 to 15 rpm.**

However, the conductivity measurements showed a trend upward as the temperature increased. Converted to conductivity from Equation 1, the results are shown in Figure 42, although only the second set of data at 225ºC is plotted. The conductivity was also slightly

higher at higher screw rates at each temperature. Unfortunately, the best conductivity was created when the material showed the most “shark skinning”, so these conditions may not be useable for co-extrusion.

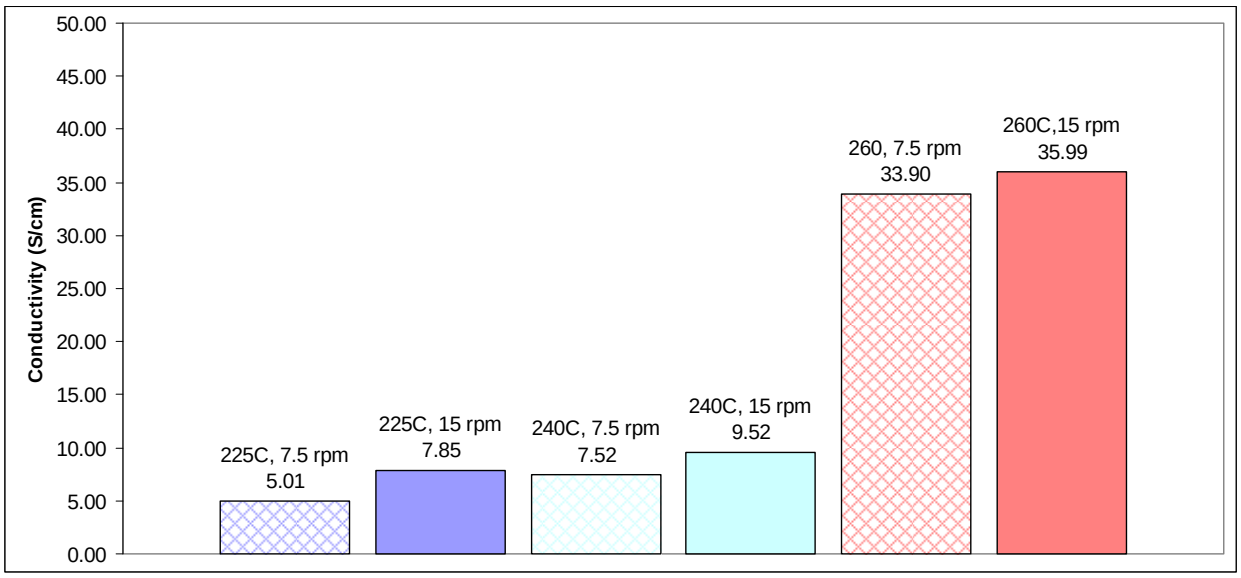


**Figure 42. Conductivities of extrudate as a function of processing condition (the value is written above each bar).**

In the end, all of the material processed was pelletized and the pellets mixed together for use in the co-extruder.

# 4 DEVELOPMENT OF A FILLED DIELECTRIC POLYMER

In order to both improve the dielectric properties of the polymer and better match the viscosity and density of the conductive layer, we decided to fill the polystyrene with barium titanate ($BaTiO_3$) powder (diameter >2 μm), a material with a very high dielectric constant. For example, polystyrene typically has a dielectric constant of 2.4-3.0, whereas $BaTiO_3$ can have a dielectric constant from 100-1250 (Computer Support Group 2009). The $BaTiO_3$ has a density of 6.08 g/cm$^3$, less than that of the nickel and eutectic (8.91 and 8.55 g/cm$^3$, respectively), but still much higher than that of polystyrene (1.05 g/cm$^3$ ). We expected that the viscosity of the eutectic mixture would be less than that of the same volume percent of solid particles, and from past experience, we also expected that we could not process a material much over 40 volume % solids. Therefore, we did not expect to match both the density and viscosity of the two filled materials, but only to come closer using $BaTiO_3$ as a filler than if using unfilled polystyrene as the dielectric material. Also, the $BaTiO_3$ powder was sticky and proved hard to process. Nevertheless, samples of 20 volume % and 30 volume % $BaTiO_3$ in polystyrene were mixed in the Minilab and tested for capacitance. The effective dielectric constant was measured using an Agilent 16451B Dielectric Test Fixture. This measurement included a contact resistance, so it is not an exact value of the material property, but rather a good indication of the relative change from one material to another. The 30 volume % material showed an increase in this effective dielectric constant of about 20% over that of the neat polystyrene material, assuming the contact resistance did not change significantly (Figure 43) [Lester 2009].

Another idea to create a better dielectric material that better matched the density of the conductive material was to use the nonconductive submicron nickel particles as a filler. As also

shown in Figure 43, this proved to be a viable option at higher particle loading based on the measured dielectric constant.

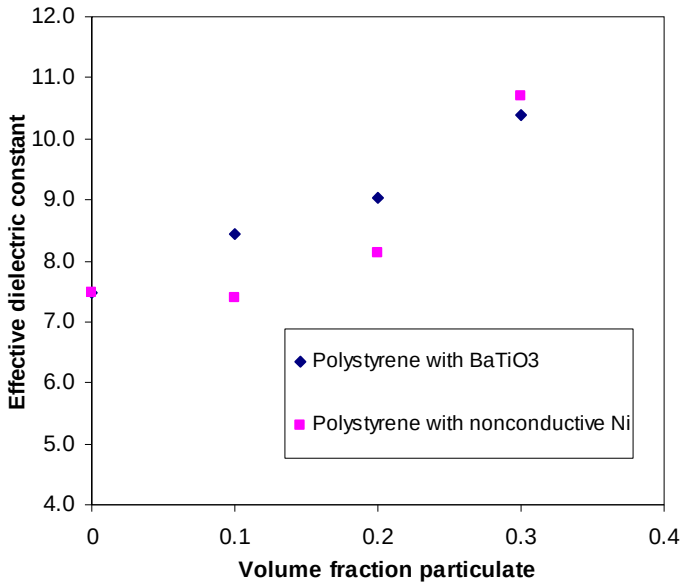


**Figure 43. Effect of filler addition on the dielectric properties of polystyrene**

Unfortunately, the results of the dielectric constants did not come in time to make a large batch of the nonconductive submicron nickel particles in polystyrene for use in co-extrusion. Furthermore, due to time constraints, there was no time to test the viscosity of any of these filled materials before processing with the co-extruder. Had there been, we could have adjusted the formulation of the dielectric to better match the viscosity of the conductive material.

Without prior knowledge of the rheology of the filled polymers, we used equation 1 to obtain an educated guess of what volume fraction $\phi$ of BaTiO3 to use to match the viscosity of the nickel-eutectic-polystyrene conductive formulation (that we had already chosen, as described in the last section). We also used an educated guess of the viscosity of the conductive material based on equations 1 through 4 and a mixture relationship for the viscosity of the conductive emulsion/suspension material. The mixture relationship was based on work by Farris for suspensions of mixtures of two particle sizes [Farris 1968]. Like Farris, we assumed that the

relative viscosity of the mixture could be considered the same as the relative viscosity of the solid particles in a continuous phase that was represented by the viscosity of the emulsion without the solid particles. In other words, the relative viscosity of the nickel-eutectic-polystyrene mixture, $\eta_{Ni-eu}/\eta_0$, would be the relative viscosity of the suspension of nickel particles alone times the relative viscosity of the eutectic droplets alone, or, for low shear rates

$$\frac{\eta_{Ni-eu}}{\eta_0} = \frac{\eta_{Ni-eu}}{\eta_{eu}} \frac{\eta_{eu}}{\eta_0} = \left\{ (1 - \frac{\phi_{Ni}}{\phi_m})^{-[\eta]\phi_m} \right\} \left\{ 1 + \phi_{eu} + 2.5\phi_{eu}{}^2 \right\}, \qquad \textbf{7}$$

and for high shear rates

$$\frac{\eta_{Ni-eu}}{\eta_0} = \frac{\eta_{Ni-eu}}{\eta_{eu}} \frac{\eta_{eu}}{\eta_0} = \left\{ (1 - \frac{\phi_{Ni}}{\phi_m})^{-[\eta]\phi_m} \right\} \left\{ (1 + \phi_{eu} + 2.5\phi_{eu}{}^2)(\frac{3 + 12\phi_{eu}}{3 + 20\phi_{eu}}) \right\}, \qquad \textbf{8}$$

where $\phi_{Ni}$ = 0.12 and $\phi_{eu}$ = 0.28. The predicted values, which will be shown in the next section in Figure 48, led us to try to co-extrude our conductive metal-filled polymer with a dielectric layer of 20 to 25 volume % $BaTiO_3$ in polystyrene. The co-extruder processing proceeded in parallel to the viscosity measurements discussed in the next section.

# 5 RHEOLOGY OF THE FILLED POLYMERS

## 5.1 Conductive material

The rheology of the candidate conductive material (12 volume % nickel, 28 volume % eutectic, and 60 volume % polystyrene) was measured with both a shear sweep using parallel plates on an TA ARES controlled strain-rate rheometer and on a Dynisco LCR 7000 capillary rheometer. With the capillary rheometer, we obtained data at higher shear rates. Because the materials were all shear thinning, a Rabinowitsch correction [Barnes et al. 1989] was used for all data sets reported here. Figures 44 and 45 show the shear thinning nature of the neat polystyrene and the metal filled system. The decrease in viscosity with increasing temperature is also evident.

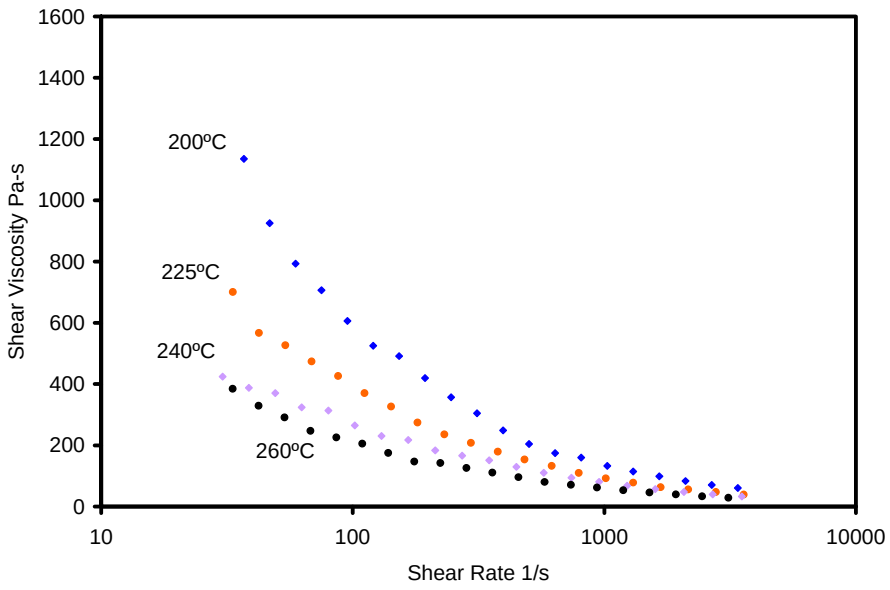


**Figure 44. Neat polystyrene capillary rheometry measurements.**

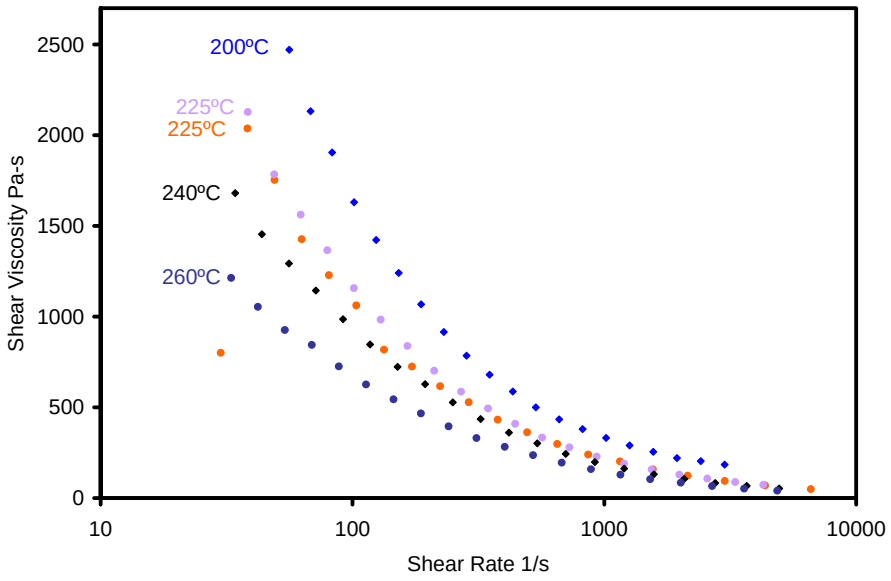


**Figure 45. Capillary rheology measurements of the 12 volume % nickel, 28 volume % eutectic, and 60 volume % polystyrene.**

Lower shear rates were measured with the ARES using 25 mm parallel plates and a nominal gap height of 1.5 mm. The data from the parallel plate geometry at 225ºC is shown in Figure 46 superimposed on the capillary rheometer data at the same temperature. It was impossible to obtain useful data above a shear rate of 1 $s^{-1}$ with the parallel plate geometry. The slight disconnect in the two sets of data could be because of slip at the wall or simply because of the nature of the polymeric and multiphase materials, which can exhibit different microstructures in different shear geometries and regimes. A serrated plate was used with the neat polystyrene because it appeared to be slipping more than the particle loaded material. Standard procedures to test for slip includes looking at different gaps between plates with the ARES and different bore diameters with the capillary rheometer. Unfortunately, there was not enough spare conductive material to look at multiple samples in various geometries. In the parallel plate we only had enough material for one sample. It was observed that the shear history seemed to change the apparent viscosity, so we report the initial data and did not examine various temperatures.

Interestingly, in the capillary rheometer, repeated tests on the same sample did not change the results significantly. With this rheometer we don't expect to have as significant an effect on the microstructure of the suspension as can occur during shear between parallel plates, nor do we expect settling of the particles that could occur in the parallel plate geometry. However, because of time constraints, we only looked at the effect of changing the bore size with the dielectric material, as reported in the next subsection.

Finally, the conductive material appears much more shear thinning than the neat polystyrene, contrary to the theory outlined in Sections 3.1 and 4 (equations 1-4 and 7-8). This will be discussed again in the next section.

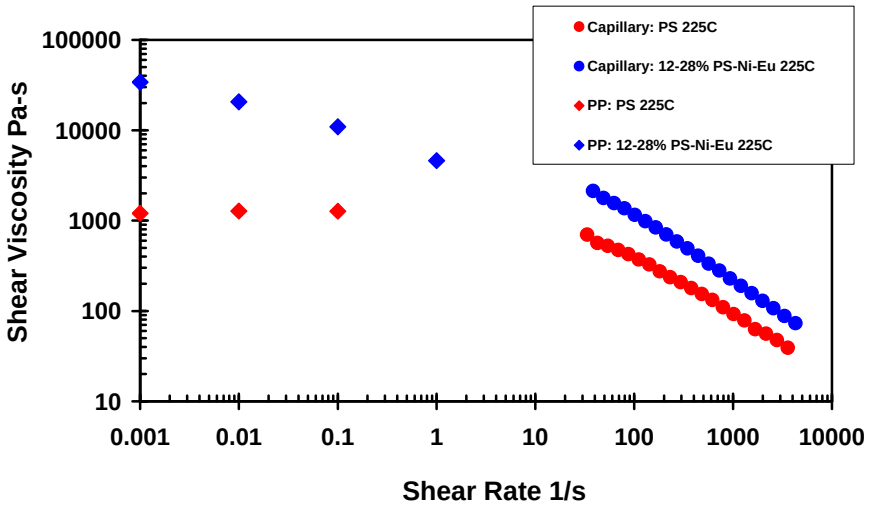


**Figure 46. Comparison of rheology tests with parallel plate and capillary geometries**

## 5.2 Dielectric material

Polystyrene samples filled at three volume fractions of $BaTiO_3$ were also tested with one or both rheometers. Results (Figure 47) show that the material was not very sensitive to the volume fraction of solids between 20 and 30%. The parallel plate and small bore capillary rheology matched fairly well. However, when the large bore was tested with the suspension of

25 volume % $BaTiO_3$, the sample showed classic "stick-slip" rheology [Macosko 1994]: The data sets consistently each contained a large discontinuity as shown in Figure 47. Clearly, more tests would be useful to understand the rheology of these complex multiphase systems.

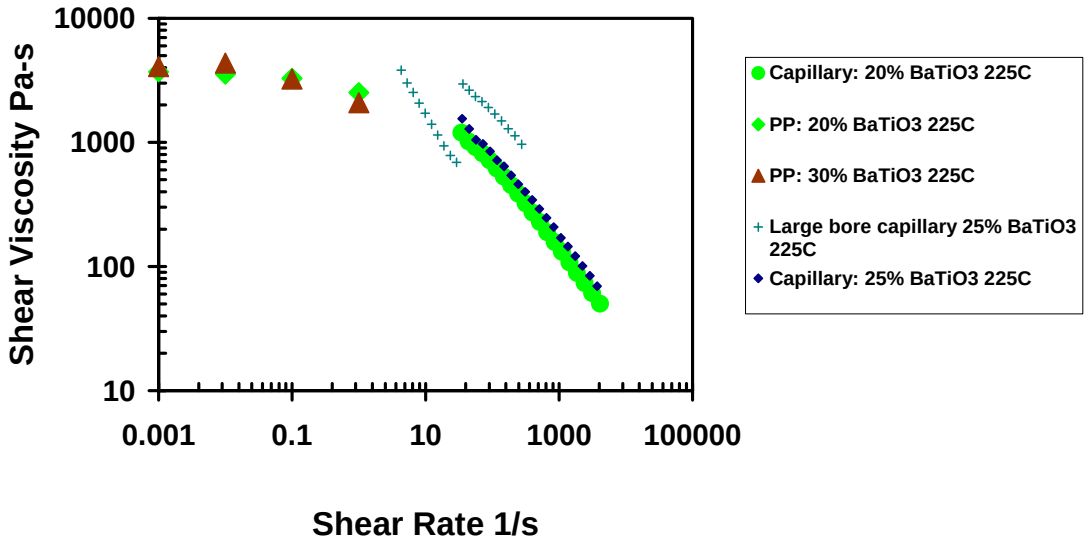


**Figure 47. Rheology of the $BaTiO_3$-filled polystyrene systems in capillary and parallel plate (PP) geometries.**

The concentration range to use for the initial co-extrusion test was estimated based on the equations outlined in Section 3.1, as previously discussed in Section 4. Figure 48 shows that although the estimated viscosities of the $BaTiO_3$-filled polystyrene were only somewhat inaccurate at the higher shear rates of the capillary rheometer, the measured viscosities of the $BaTiO_3$-filled polystyrene at lower shear rates were higher than expected. Again, at the highest shear rates the estimate of the conductive material's viscosity (equation 8) was reasonable. However, the viscosity of the conductive material was so much higher at lower shear rates than expected that the mismatch between the conductive and nonconductive phases were extreme at the lowest shear rates tested.

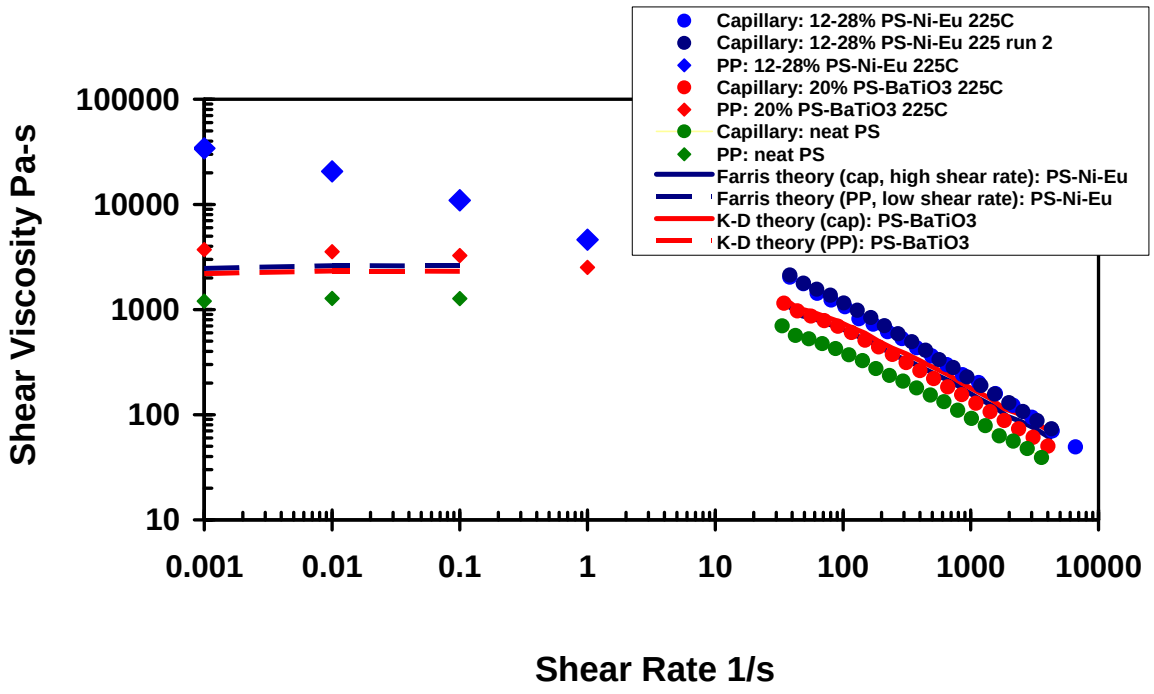


**Figure 48. Combined plot of the rheology measurements of the conductive material (labeled PS-Ni-Eu) and the dielectric (labeled PS-BaTiO3) and the theoretical predictions (equations 1, 7-8).**

# 6 CO-EXTRUSION OF FILLED SYSTEMS TO MAKE A CAPACITOR

The final conductive material (12 volume % of nickel, 28 volume % of eutectic, and 60 volume % of polystyrene) and a dielectric material made of 25 volume % $BaTiO_3$ in polystyrene were co-extruded to form an 8-layered structure. As shown in the next section, these materials were not ideal from the standpoint of flow stability. The density and viscosity mismatches were far from optimal. Although we believe we know now how to achieve a much more stable system, we tested these materials as a proof of principle. Furthermore, we believe we could make a much better conductive material for future tests.

The co-extruder can be run at various flow rates (screw RPM), with each material independently controlled. Other processing parameters include temperature and the take up rates of the two chilled rollers. A complete design-of-experiment would include a matrix of values for the parameters. The goal of this proof-of-principle experiment was merely to get experience running filled polymers and to see if the final layered structure could be useful as a capacitor.

In our minimal testing, we found that, contrary to our estimate from our experience processing in the twin-screw and the preliminary rheology measurements, the co-extruded material looked better at lower flow rates. This was primarily due to bubble formation at the drawdown, a phenomena not seen in our co-extrusion with neat polymers. Bubbles that extended through the thickness of the extruded ribbon would appear at the exit and the pull of the take up rollers would stretch them into significantly large voids (Figure 49). Running at higher temperatures (260ºC as opposed to 235ºC) made the voids more numerous. We believe that the bubble formation was augmented by the presence of solid particles. The bubbles could have been formed from cavitation, but we think it more likely that they formed from air entrained during

incorporation of the particles into the polystyrene or from de-adhesion of the polystyrene from the particles. Flowing at a significantly lower rate minimized the bubble formation and prevented stretching of the remaining bubbles; however, the motors on the take up rollers could not run at that low rate. A simple modification to the equipment would be necessary before continuing these studies.

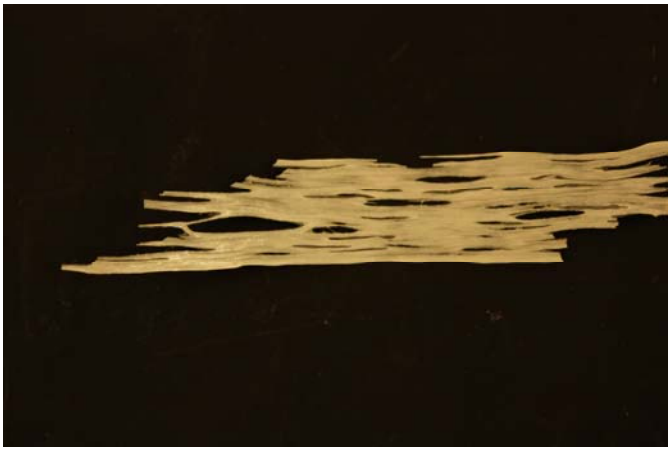

**Figure 49. View looking down at the top dielectric layer of the ribbon co-extruded at 40 rpm and 235ºC. Bubbles have created large tears in the ribbon.**

When the exit temperature was cooled to 200ºC and the flow of the two materials were regulated so that the higher viscosity conductive material was pushed at twice the rate of the lower viscosity dielectric material (20 and 10 rpm respectively) a fairly nice layered ribbon was formed. An SEM of a random representative sample of this ribbon is shown in Figure 50. These rates were still too high to fully eliminate the bubbles as can be seen in the figure as dark spots. They seem to appear here only in the conductive layer. Although pushing the materials at different rates, according to the ratio of their viscosities, improved the layer formation, a flaw can still be seen near the top. The large aggregates (white) in the SEM are probably eutectic droplets; however, we were unable to get a spectra in the time allotted to confirm this. A higher magnitude image of a different section of ribbon is shown in Figure 51.

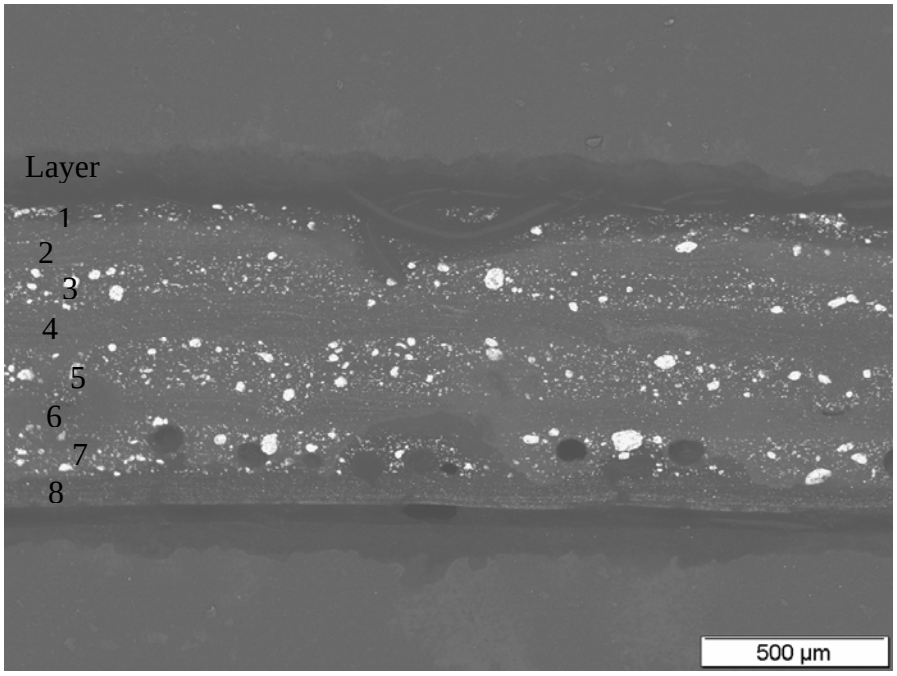


**Figure 50. Cross-section 50X SEM of layered structure formed at an exit temperature of 200 ºC, where the conductive layer is extruded at 10 rpm and the dielectric at 20 rpm.**

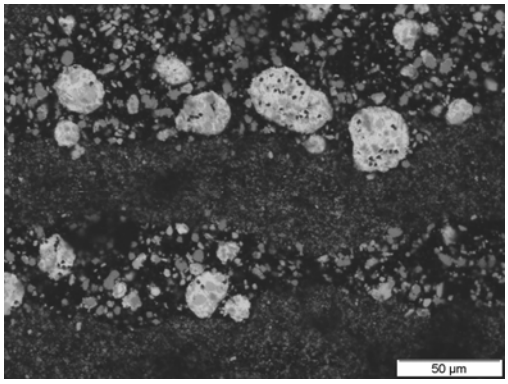


**Figure 51. Cross-section 500X SEM of four layers in the 8-layer ribbon.**

The resistance per length of the exposed surface conductive layer was measured to be between 1000 and 2000 Ohm/cm and that of the exposed dielectric layer had no measurable conductance. A capacitor measurement was performed by treating the structure as a 2-plate capacitor using a 4 wire bridge type capacitance measurement. By connecting the 4 wire bridge capacitance meter to the aforementioned conductive surfaces and piercing through the opposing

non-conductive surface until conductive material was touched, a capacitance measurement of 275 pF and a dissipation factor (DF) of 0.5 was recorded. The large DF number is due to the high internal resistance of the structure, whereas a DF of 0.005 would be a more realistic number for a good capacitor.

# 7 FINITE ELEMENT MODELING

The goal of our modeling work was to develop a numerical capability suitable for optimizing and troubleshooting the co-extrusion process and circumventing flow instabilities such as ribbing, barring, and encapsulation that can lead to variable layer thickness and a poor quality extrudate [Dooley and Rudolf 2003, Rincon et al. 1998]. Details of the modeling approach and equations, the numerical methods used and the finite element implementation, and the complete results can be found in another report [Rao et al. 2009]. We will only summarize the results here.

A numerical model of a multilayer co-extrusion process has been developed based on a finite element discretization and two different free surface algorithms: an arbitrary-Lagrangian-Eulerian (ALE) moving mesh implementation and an Eulerian level set method. The free surface algorithms help us to understand the moving boundary problem associated with the polymer-polymer interface. For this study, elastic instabilities are ignored and we focus on Newtonian and shear-thinning fluids only.

Numerical models of varying degrees of complexity were investigated including stability analysis and direct finite element free surface approaches. Linear stability analysis was used in simplified two-dimensional geometries to help understand the limit on density mismatch between layers. Finite element free surface flows were used in three different three-dimensional (3D) geometries to understand stable operating conditions such as pressure or flow rate mismatch or viscosity mismatch and to examine a novel die design that allows for offsets between layers. The three geometries we examined are:

1. Flow in an offset die, designed to have one polymer encapsulate another.

2. Flow through the splitter where the number of layers is doubled by vertically slicing the flow and then restacking it.
3. Flow in a converging die, where an initially square cross-section is drawn down to a tape with the same area, but having a thinner, wider cross-section.

Here we will only summarize the second geometry and discuss the implications of the results in terms of creating a layered structure for a capacitor with our filled systems.

3D free surface flows can give us a great deal of information about the shape of the extrudate and how materials properties and processing parameters affect final film thickness and distribution. Because of the complexity of the numerical approaches and because boundary conditions at the wall were not known, an important goal was to validate a model with experimental data. We undertook simulations on a simplified model of a two-layer structure split and multiplied to be a four-layer one (Figure 52).

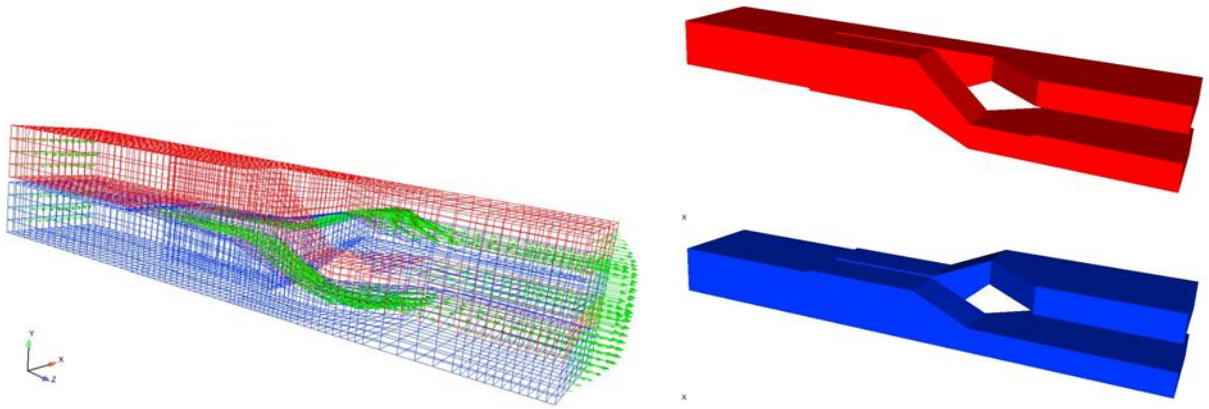

**Figure 52. Co-extruder mesh for initial multiplication creating a four-layered structure by splitting and restacking a two-layered one. Velocity vectors on mesh (left) show acceleration and redirection of fluid through the splitter. The view on the right shows a break out of the two fluids to more clearly see the splitter design.**

Both ALE and level set simulations were done. In the ALE simulations we specified no slip at the wall. The inherently transient nature of the level set simulation introduces some slip

at the wall, even when no slip is applied, since the interface location evolves in time. We wanted to determine which boundary condition was more appropriate: slip or no slip. To this end, we undertook a validation experiment to look at materials with the same density and viscosity and run at the same flow rate. To differentiate the two polymers, we added 3 volume % carbon black to create a black material and 3 volume % titanium dioxide to the other layer, to create a white material. This was an amount suitable to change the color of the polymer without significantly affecting their properties. Results from the validation experiment are given in Figure 53.

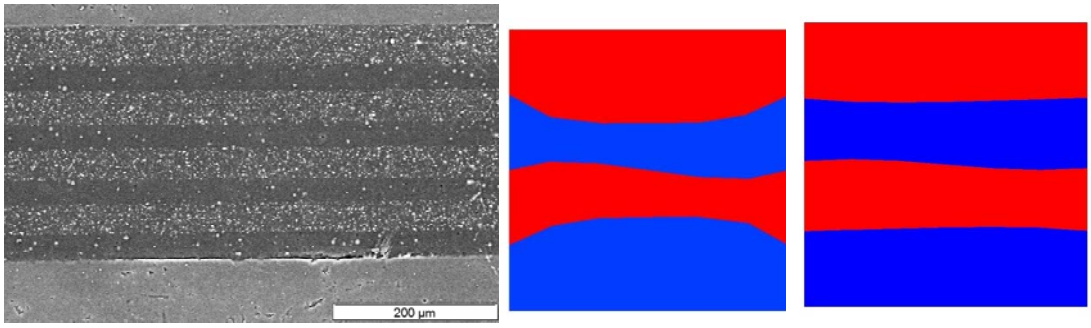


**Figure 53. Comparison of black and white experiment SEM (left) to ALE result (middle) to level set result (right) for the same properties and inflow pressure (10,000 dyne/cm$^2$). The red and blue phase properties are equal at 10,000 Poise and 1 g/cc. The interfacial tension between layers is assumed to be 45dyne/cm$^2$.**

From this validation experiment, it was determined that some slip does occur at the walls during co-extrusion and that either running transient with the level set formulation or using a slip boundary condition with ALE is preferable to steady simulations with no slip. Therefore, the following results all include slip at the boundary.

When we increased the injection rate of the red material over that of the blue with a pressure mismatch, the results showed thinner layers of the slower flowing material (Figure 54). Here the red and blue materials once again had equal properties. SEMs of the experiment in

which the ratio of the extrusion speed of the carbon black to that of the titanium dioxide was mismatched is shown in Figure 55, where one can see that the layers start to lose integrity.

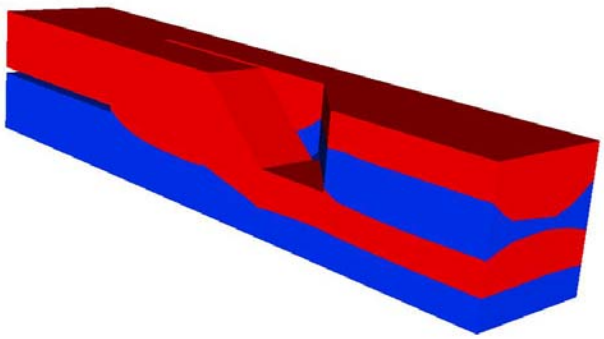

**Figure 54. Pressure mismatch creates thinner layers of the slower flowing material (blue). Ratio of red to blue pressure =1.76.**

a b

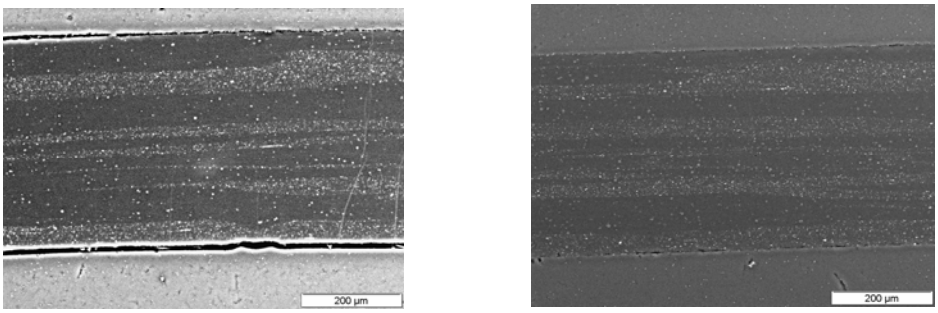


**Figure 55. a) SEM of co-extruded material shows distortion of layers at a ratio of flowrate = 1.5. Here light is equivalent to blue in the model in Figure 53. b) At higher ratio (1.75) layers lose integrity and mixing begins.**

We used the level set method to investigate property ratios and processing parameters that we could not reach with moving mesh methods. Figure 56 shows results for an equal order, but higher inflow pressure (100,000 dyne/cm$^2$) and equivalent properties. For this inflow pressure, we see distortion of the red fluid sandwiched between the two layers of blue fluid. If we increase the viscosity ratio between fluids by making the viscosity of the red fluid 10 times that of the blue fluid, we see that we get total encapsulation of the red fluid by the blue and loss of the layered structure as the two blue layers coalesce.

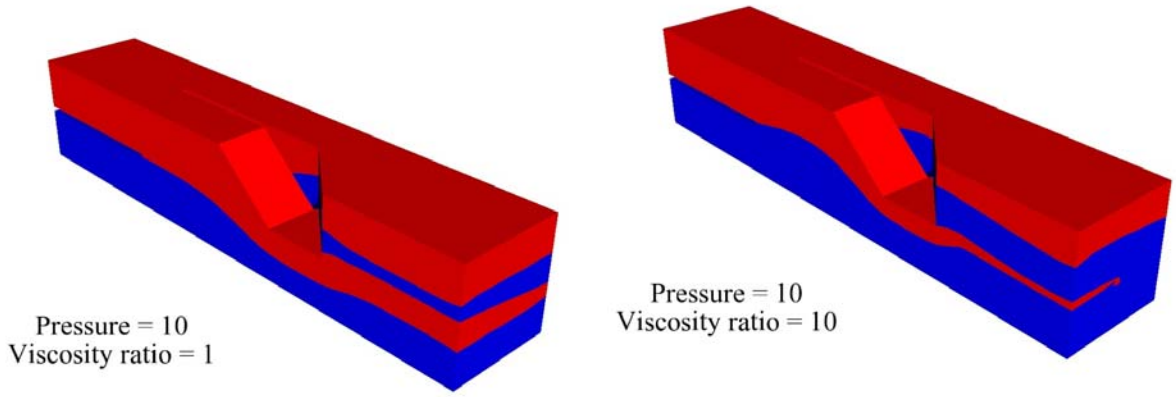


**Figure 56. Comparison of level set results for the same properties and inflow pressure (100,000 dyne/cm$^2$) (right) with level set results for red phase viscosity of 100,000 Poise with blue phase viscosity at 10,000 Poise (left). Both densities are held constant at 1 g/cc. The interfacial tension between layers is assumed to be 45 dyne/cm$^2$.**

As we came closer to a material down selection, we wanted to understand how the stability of the flow would be affected by both dissimilar densities and viscosities. For this case, we use a red phase viscosity of 25,000 Poise and density of 4.09g/cc to represent the conductive polymer, which is a mixture of 12 volume % Ni particles and 28 volume % eutectic in polystyrene. The blue phase viscosity was assumed to be 15,000 Poise and the density to be 2.06g/cc to represent the dielectric, which is a composite of 20% $BaTiO_3$ ceramic particles in polystyrene. Both filled-polymer systems are shear-thinning, but we assumed they are Newtonian for this study, and estimated their viscosities from the early conductive phase data at 60 sec$^{-1}$ and a guess at the (at the time unmeasured) dielectric viscosity based on a Krieger-like analysis [Gupta 2000]. Because the polymer matrix is the same in both phases, we assume that there is no interfacial tension between the phases. The results from this test case are given in Figure 57.

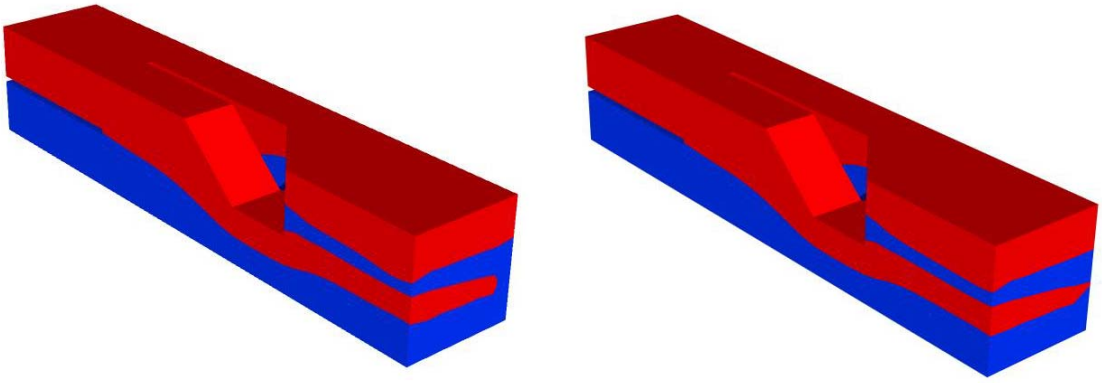

**Figure 57. Level set simulations for the estimated properties for the conductive red phase (25,000 Poise, 4.09g/cc) and dielectric blue material (15,0000 Poise, 2.06g/cc). The inflow velocity is 5 cm/s. The picture on the left shows the simulation at an early time when the bottom red sheet breaks. The picture on the right shows it reforming at later times, which ends up being the steady profile.**

From Figure 57, we can see that the combination of mismatched viscosity (ratio = 1.667) and mismatched density (ratio = 1.99) results in problems in the splitter where the conductive red fluid can become encapsulated by the lower viscosity blue dielectric fluid, and the bottom red layer breaks and then reforms in the steady solution. The actual viscosity mismatch of the real materials turned out to be much bigger, and the layer formation greatly flawed when the materials were extruded at the same rate. Oscillations occur in the numerical solution where we see waves in the bottom meniscus reminiscent of Rayleigh-Taylor instabilities. Because we were interested in short turn-around-times for the simulation, a relatively coarse mesh was used. In future, we recommend revisiting these simulations with a finer mesh.

This new finite element capability has shown promise in being able to predict property ratios and flow rates at which the co-extruded layers would be unstable. We believe this tool will greatly increase our chance of significantly improving the quality of multilayered material formed with our co-extruder.

# 8 DISCUSSION AND CONCLUSIONS

The basic goals of the project, to create a co-extrusion capability at Sandia National Laboratories and to explore the possibility of co-extruding filled systems, were achieved. A new conductive material was created and characterized, which has potential applications beyond capacitors in other areas such as soldering. Not only did the co-extruder itself create new capability, but the project was leveraged to bring in new capital equipment in the form of two twin-screw extruders. A new, unique, numerical modeling capability in three-dimensional, complex, free-surface flows and stability analysis, as well as a better understanding of processing filled polymers also resulted from this project.

There are many improvements possible to the current primitive co-extrusion capability. Basic design changes in the equipment could be a first start. The current splitter dies have abrupt blunt edges. Knife edges would improve flow stability. The rollers need to be mobile so that they can be brought in closer if all of the sections are not used. The roller motors need to be geared down to allow slower flow rates.

Even more important than minor changes in the equipment would be improvements in the materials. Although the early studies on using a eutectic to form an emulsion rather than solid particles were promising, much work remains in order to optimize the formulation and improve the incorporation of the eutectic. Fundamental studies on process control of droplet size formation would be advised to aid in reducing droplet size for use in fine layers. Using only solid materials could be a viable alternative if the size distribution could be improved to lower the viscosity. For example, bimodal, trimodal, and even higher modal size distributions have been used for decades in propellant formulations to achieve very high particle packing while

maintaining processability [Farris 1968]. Nanoparticles were not explored in this LDRD because of cost, schedule, and the time needed to satisfy ES&H requirements when using nanoparticles. However, looking at a range of other conductive particles including carbon nanotubes is strongly advised since these materials percolate at much lower volume fractions and have the possibility of remaining flexible in the final part. Using smaller particles would allow for much thinner layers, greatly enhancing the possible range of capacitance, for example. From a material development standpoint, we should also investigate different polymeric suspending fluids. The polystyrene used here had a high viscosity and was extremely shear-thinning, resulting in a composite material that followed these properties. Using a low molecular weight polyethylene would have resulted in a superior rheology for co-extrusion and less likelihood of cavitation. In addition, using different polymers for the conductive and dielectric phase polymer matrix would stabilize the layers by introducing an interfacial tension between layers and reduce mixing between the layers. Finally, another suggestion would be to use only a eutectic as the conducting phase, although that would undoubtedly have its own material challenges.

One important idea to explore is the addition of processing aids such as surfactants used as dispersive agents. [Yang 2009, Huang and Cheng 2009]. It has been found that such dispersive agents can allow much higher concentrations of particles to flow smoothly by dispersing the particles, adhering them more strongly to the polymer matrix, and reducing the viscosity of the composite system.

Rheology measurements have proved to be critical to determining the final quality of the co-extruded part. Once we had measured the shear-dependent rheology of the conductive and dielectric material it became clear that the viscosity mismatch of 10 between the two phases would lead to flow instabilities. These problems were seen when we co-extruded the material.

Numerical modeling has also been valuable for elucidating optimal processing regimes from viscosity and density mismatch to flow rates.

In this project, we have developed the science behind creating conductive and processable filled-systems for co-extrusion applications. With relatively minor changes to the process and the materials, we feel that we could produce a useable capacitor. The great advantage of the co-extrusion process is that large amounts of materials can be made very quickly. Our rate of production was greater than 1 cm/s of ribbon. The ribbon is malleable until cooled, so can be bent, twisted, or rolled into a variety of final geometries. Furthermore, the method is not limited to creating sheets of material, as dies can be made to extrude other shapes. Thus, we feel that there is a broad range of other applications that could benefit through the production of multi-functional layered devices with co-extrusion of filled polymers. A brief listing of these could include barrier materials, sensors, and batteries. For example, it may be that a thin film thermal battery could be made with co-extrusion, which would greatly reduced solvent use to produce a "greener" process.

# 9 REFERENCES


3M, 2005, "Multilayer coextrusion die and method," U.S. Patent 6837698

Barnes, H. A.; Hutton, J. F.; and Walters, K., 1989, *An Introduction to Rheology*, Elsevier, New York, p. 32.

Chung, D. D. L., 2001, *Carbon*, **39**, 279-285.

Computer Support Group, 2009, http://www.csgnetwork.com/dieconstantstable.html

J. Dooley; L. Rudolf *PFFC online.com*, Jan. 2003, 73.

Dow Global Technology, 2007 "Multilayer polymer sheets," U.S. Patent Application 20070184259.

Einstein, A., 1906, *Annalen der Physik*, **19**, 289-306.

Einstein, A., 1911, *Annalen der Physik*, **34**, 591-592.

Farris, R. J., 1968, *Trans. Soc. Rheol*., **12**, 281-301.

Frankel, N. A. and Acrivos, A., 1970, *J. Fluid Mech*. **44**, 65-78.

Gerard, M.; Chaubey, A.; Malhorta, B. D., 2002, *Biosens. Bioelectron.*, **17**, 345-359.

Gleissle, W and Hochstein, B, 2003, *J. Rheol*. **47**, 897-910.

Grizzuti, N.; Buonocore, G.; Iorio, G., 2000, J. Rheol. 44, 149-164.

Gupta, R. K., 2000, Polymer and Composite Rheology, 2nd Edition, Marcel Dekker, New York, p. 229.

Huang, C. K. and Cheng, F. S., 2009, *Intern. Polymer Processing*, **XXIV**, 267-271.

Kalyon, D. M.; Birinci, E.; Yazici, R.; Karuv, B.; and Walsh, S., 2002, *Polymer Eng. Sci.*, **42**, 1609-1617.

Khomenko, V.; Frackowiak, E.; Beguin, F., 2005, *Electrochim. Acta* **,50**, 2499-2506.

Krieger, I. M. and Dougherty, T, 1959, *Trans. Soc. Rheol.*, **3**, 137-152.

Lester, Adam, 2009, Sandia National Laboratories Organization 1732, personal communication.

Macosko, C. W., 1994, Rheology: Principles, Measurements, and Applications, Wiley-VCH, New York, p. 244-247.

Mooney, M., 1951, *J. Colloid Sci*., **6**, 162-170.

Prud'homme, R. K. and Khan, S. A., 1996, "Experimental Results on Foam Rheology," in *Foams, Theory, Measurements and Applications*, Prud'homme and Khan, Eds., Marcel Dekker, Inc. New York.

Rao, R. R; Mondy, L; Collins, R.; Baer, T; Mrozek, R; Schunk, P. R.; Hopkins, M.; and Lenhart, J., 2009, *Finite Element Analysis of Multilayer Co-Extrusion*, SAND report, Sandia National Laboratories, Albuquerque (in preparation).

Rincon, A. J.; Hrymak, A. N.; Vlachopoulos, J., 1998, *Int. J. Numer. Meth. Fluids*, **28**, 1159.

Renardy, M., 1997, *J. Non-Newtonian Fluid Mech.* **68**, 125-132.

Tao, W. H.; Chen, C.; Ho, C. E.; Chen, W. T.; Kao, C. R., 2001, *Chem. Mater*.**, 13**, 1051-1056.

Taylor, G. I. 1934, *Proc. Roy. Soc. Ser. A.* **146**, 0501-0523.

Thomas, D. G., 1965, *J. Colloid Science*, **20**, 267-277.

Wang, Shi-Qing; Drda, Patrick, 1997, *Macromol. Chem. Phys*., **198**, 673-701.

Wessling, B., 1998, *Synth. Met.*, **93**, 143-154.

Yang, Ping, 2009, personal communication.

Zhao, R; Macosko, C. W., 2002, *J. Rheol.* **46**, 145-167.

# 10 DISTRIBUTION

| | | | |
|---|---|---|---|
| 5 | MS0346 | Lisa Mondy | 1514 |
| 1 | MS0346 | Anne Grillet | 1513 |
| 1 | MS0523 | Richard Berget | 1733 |
| 1 | MS0525 | Lothar Bieg | 1732 |
| 1 | MS0836 | Terry Aselage | 1514 |
| 2 | MS0836 | Rekha Rao | 1514 |
| 1 | MS0886 | Jim Aubert | 1822 |
| 1 | MS0888 | Regan Stinnett | 1821 |
| 1 | MS0888 | Mark Stavig | 1821 |
| 1 | MS0888 | John Schroeder | 1821 |
| 1 | MS0958 | Ben Anderson | 2453 |
| 1 | MS0958 | Mike Kelly | 2453 |
| 1 | MS0958 | Scott Spangler | 2453 |
| 1 | MS0963 | Mike Winter | 2454 |
| 1 | MS0963 | Chris Diantonio | 2454 |
| 1 | MS1305 | Duane Schneider | 1132 |
| 1 | MS0899 | Technical Library | 9536 (electronic copy only) |
| 1 | MS0123 | D. Chavez, LDRD Office | 1011 (electronic copy only) |


Sandia National Laboratories